Figure 1. A map of the southwestern USA showing the location of Moses Rock in relation to the Colorado Plateau and Navajo Volcanic Field. Though uplifted ~1.8km, the Colorado Plateau remains largely undeformed relative to the neighboring tectonic provinces (Basin and Range, Rio Grande Rift and Rocky Mountains, modified from Schulze *et al.*, 2015).

Figure 2. Photomicrographs in plane polarized light of (a) sample 12-97-53 and (b) sample 12-83-24 representative of the textural and mineralogical contrast between the 12-97 samples and sample 12-83-24. In 12-97-53 garnet is found as large and discrete crystals, while in 12-83-24 garnet forms elongate aggregates. Foliation is more pronounced in 12-97-53 and defined by zoisite which is absent from 12-83-24. (Grt=garnet; Omp=omphacite; Zo=zoisite; Rt=rutile; Ap=apatite)

Figure 3. High-contrast BSE images from samples 12-97-6 (a), 12-97-11 (b and c) and 12-83-24 (d) illustrating a variety of atoll garnet textures from Moses Rock eclogite xenoliths. Garnet cores in (a-c) are largely filled with omphacite (appears black). In (d), the garnet has been recrystallized filling the euhedral atoll (bright zone) with new garnet (various grey zones). A primary origin has been proposed for these features in the NVF eclogite xenoliths (Smith & Zientek, 1979), but no definitive textural evidence was identified in the samples presented here.

Figure 4. High-contrast BSE images of garnets: (a) 12-97-11-A and (b) 12-97-11-B, showing high- δ^{18} O cores and low- δ^{18} O rims. These core values are consistent with adoption of an altered oceanic crust protolith signatures while deviations at the rim record infiltration of a serpentinite-derived fluid. Heterogeneity in cation composition can be seen in the bright annulus just inside of the low- δ^{18} O rim in (a) relative to the prograde zoning visible in (b). Ovals mark oxygen analysis pits and are grayscale-coded for their associated oxygen isotope zone. Pits are labeled with their associated δ^{18} O value (‰,VSMOW). White flecks are residual gold coating. A traverse for cation composition and δ^{18} O from garnet 12-97-11-B is marked by a white bar A-A' in (b) and associated analyses are plotted (c). Shaded bands mark different grayscale zones visible in the associated BSE image (b).

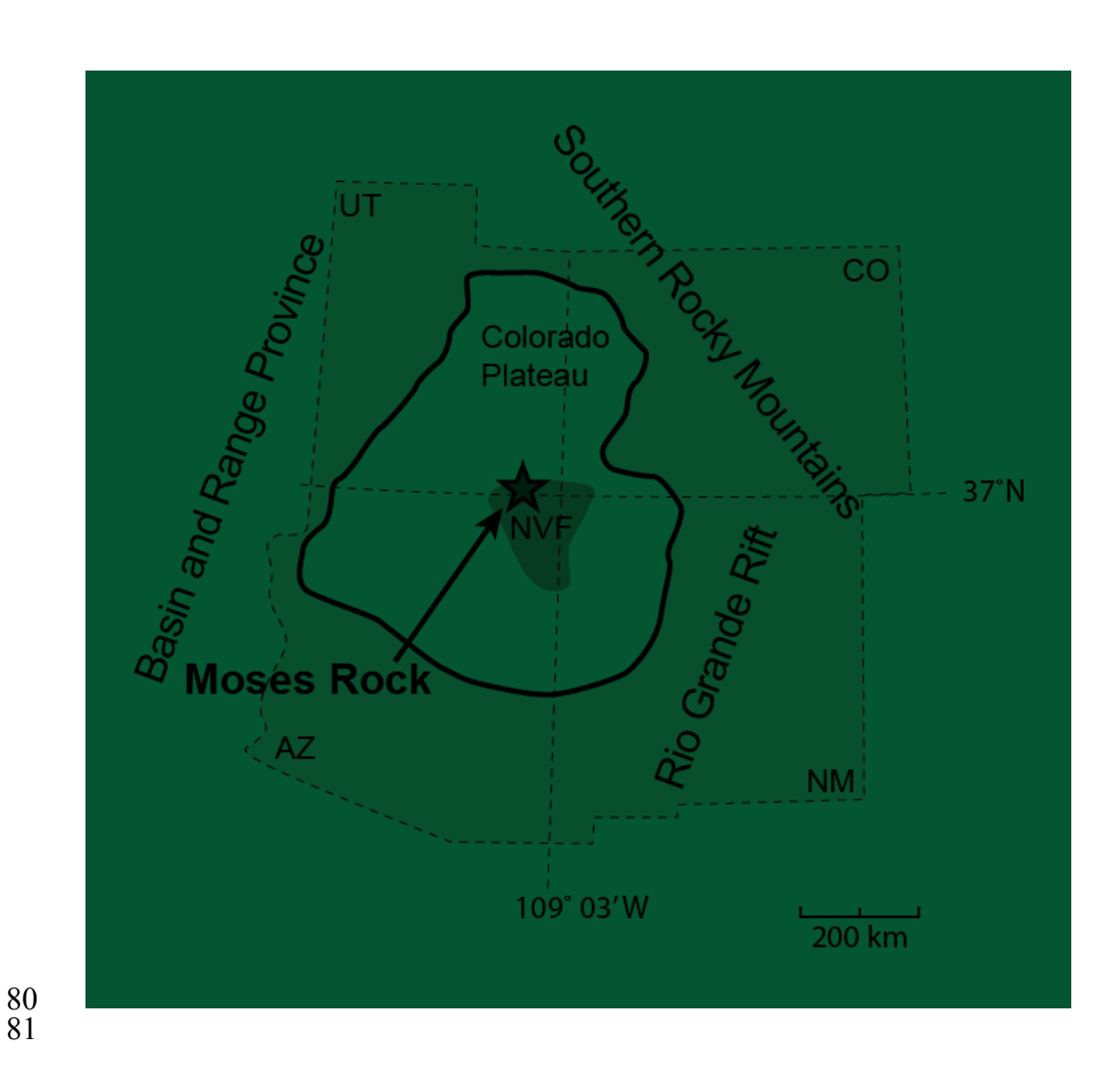
Figure 5. High-contrast BSE images of garnets: (a) 12-97-45-A and (b) 12-97-45-B, showing the heterogeneous preservation of the lowest- δ^{18} O zone. Embayed garnet rims suggest this feature is the result of garnet resorption rather than heterogeneous distribution of the serpentinite-derived fluid. Linear features cross-cutting the cores of both (a) and (b) are fractures healed with new garnet during fluid influx. Ovals mark oxygen isotope analysis pits labeled with their associated δ^{18} O value and grayscale-coded for their zone. Cation traverse A-A' is marked with a white bar in (a) and associated analyses are plotted in (c). Shaded bands refer to grayscale zones visible in the associated BSE image (a).

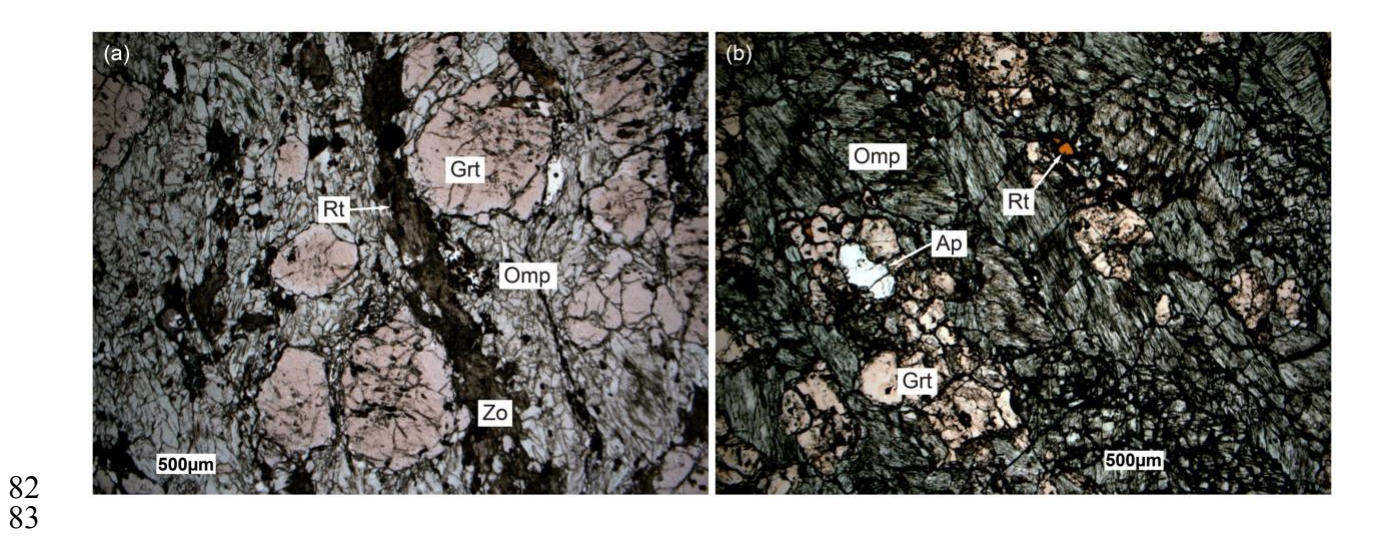
 Figure 6. High-contrast BSE images of garnets: (a) 12-97-53-A and (b) 12-97-53-B, showing $\delta^{18}O$ homogeneity but cation zoning and healed fractures indicating changing metamorphic conditions and fluid interaction during growth. The abundance of embayments in the garnet rims suggest that lack of preservation may explain the absence of a low- $\delta^{18}O$ rim zone in this sample. Ovals mark oxygen isotope analysis pits labeled with their associated $\delta^{18}O$ values (‰, VSMOW).

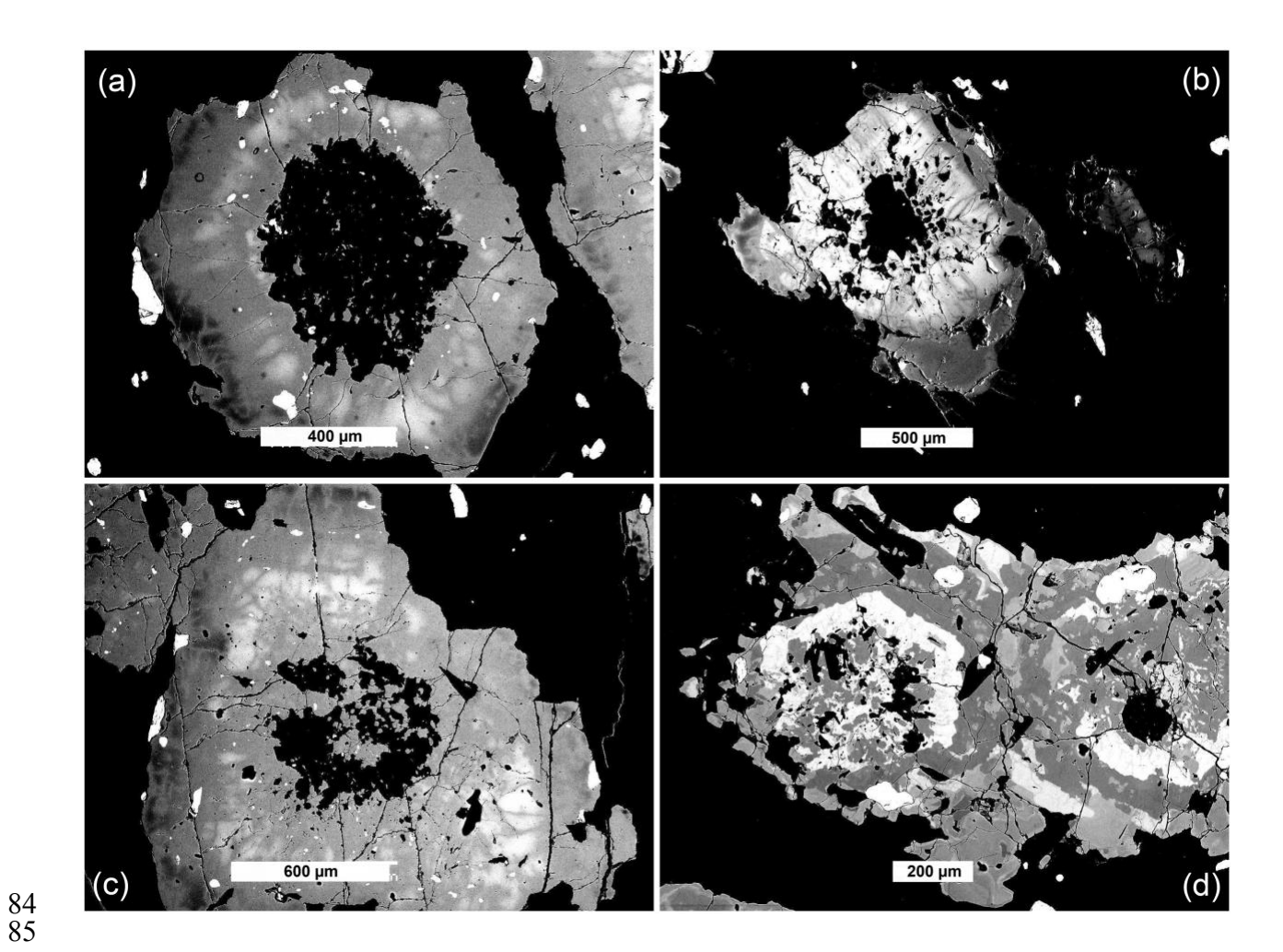
 Figure 7. (a) High-contrast BSE image of garnet 12-83-24-A showing the complex zoning characteristic of this sample. The high- δ^{18} O values in the bright zone suggest this represents first garnet growth with later diffusion-limited recrystallization forming the complex intergrowths in the core and rim. Ovals mark δ^{18} O analysis pits labeled with their associated δ^{18} O value (VSMOW) and grayscale-coded for their associated oxygen isotope zone. The cation traverse carried out for this sample is marked by the white bar from A to A'. (b) Cation and δ^{18} O analyses along traverse A-A' are plotted with other δ^{18} O values assigned a position along the traverse based upon cation chemistry and marked with an "x". Numbers and shaded bands identify zones differentiated by oxygen isotope and cation analyses. (c) Detail of the traverse portion of (A) with the relict atoll outlined. The fine-scale, complex zoning in the later low- δ^{18} O garnet is clearly visible as is the healed fracturing in the relict atoll.

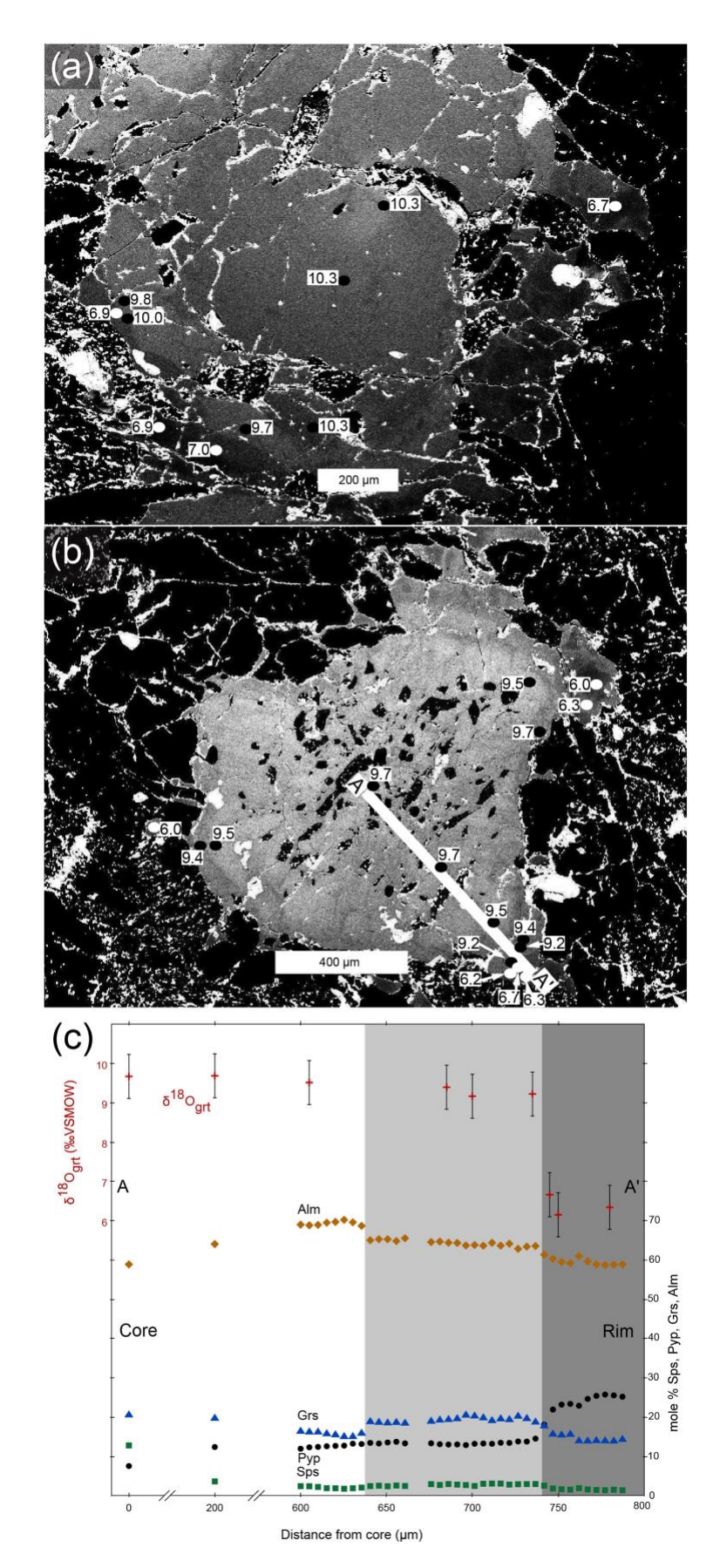
Figure 8: Representative multi-cation diffusion model results for garnet rim (12-97-45-A outside rim; a and b) and healed fracture (12-97-45-B fracture; c and d) traverses. In (a) and (c), black bars mark the position of measured traverses plotted in (b) and (d), respectively. Plotted lines in (b) and (d) are a range of diffusion models at 680°C considered good fits to the measured profiles, based on visual assessment. Variability in the models in (b) close to the zone boundary are the result of a complex initial geometry. Multiple initial steps in concentration were necessary to maximize the fit of the model to the measured data.

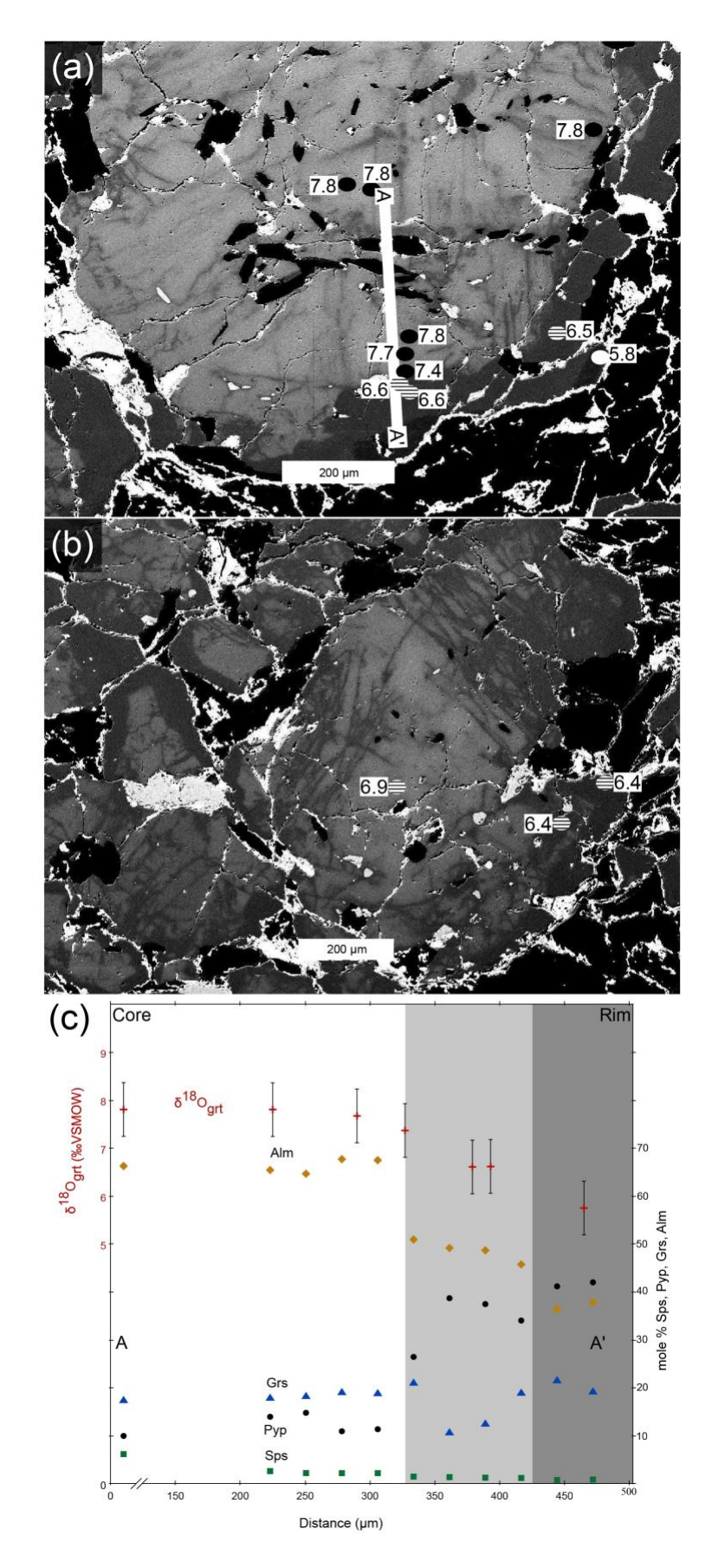
Figure 9: Compilation of oxygen isotope profiles across garnets in this study with core-to-rim distances normalized for comparison. Low- $\delta^{18}O$ zones in all samples that preserve zoning converge at values of $\sim 6.5\%$ suggesting a shared history of fluid infiltration. Based on tectonic, trace element and stable isotope arguments, this fluid is likely derived from serpentinite in the Farallon lithospheric mantle. Higher $\delta^{18}O$ values in all samples are consistent with an altered oceanic crust protolith suggesting closed system growth during prograde subduction. Mantle garnet (with 2SD uncertainty, fine dashed lines) and serpentinite (shaded region) are plotted for comparison. Analyses from sample 12-83-24 were assigned positions based on atoll and overgrowth textures.

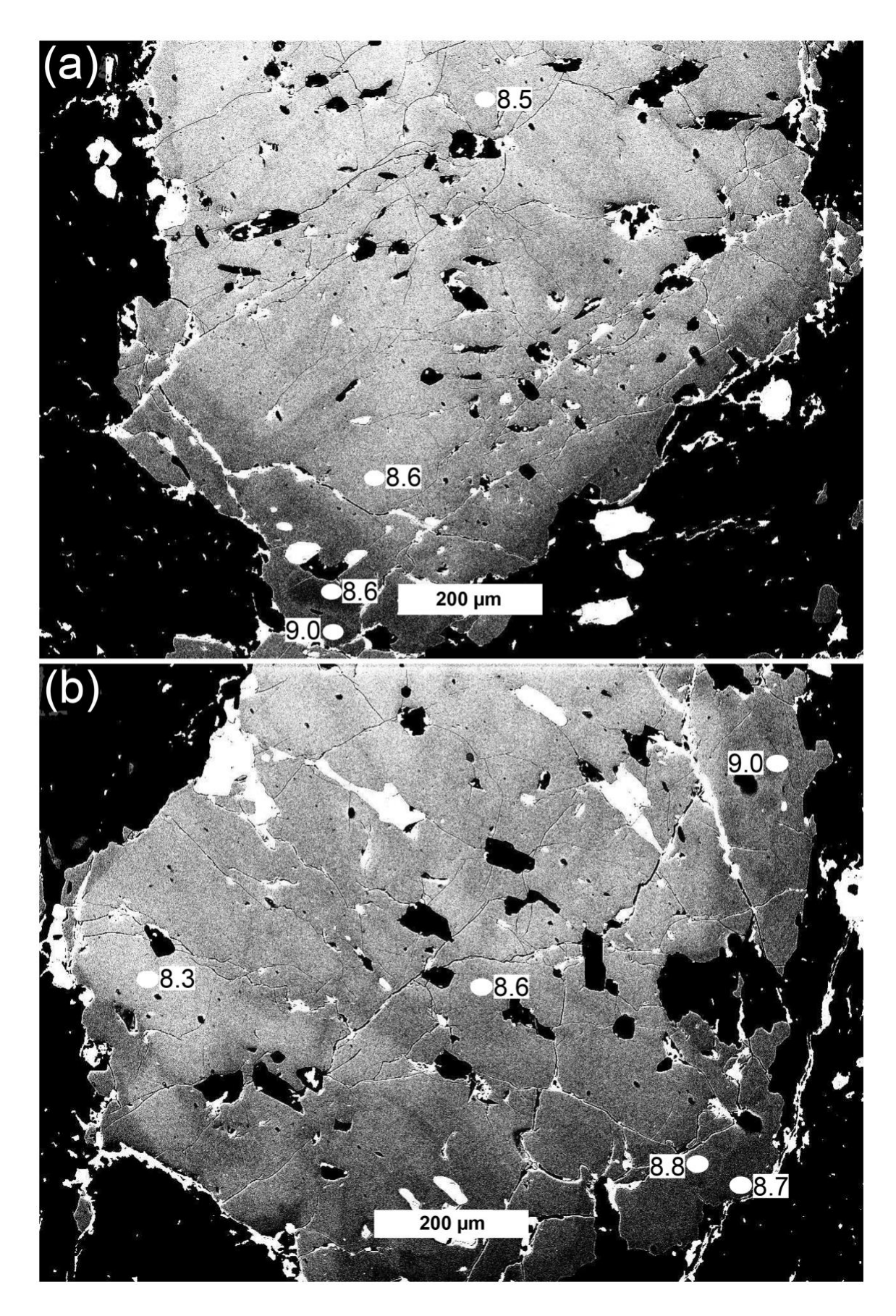


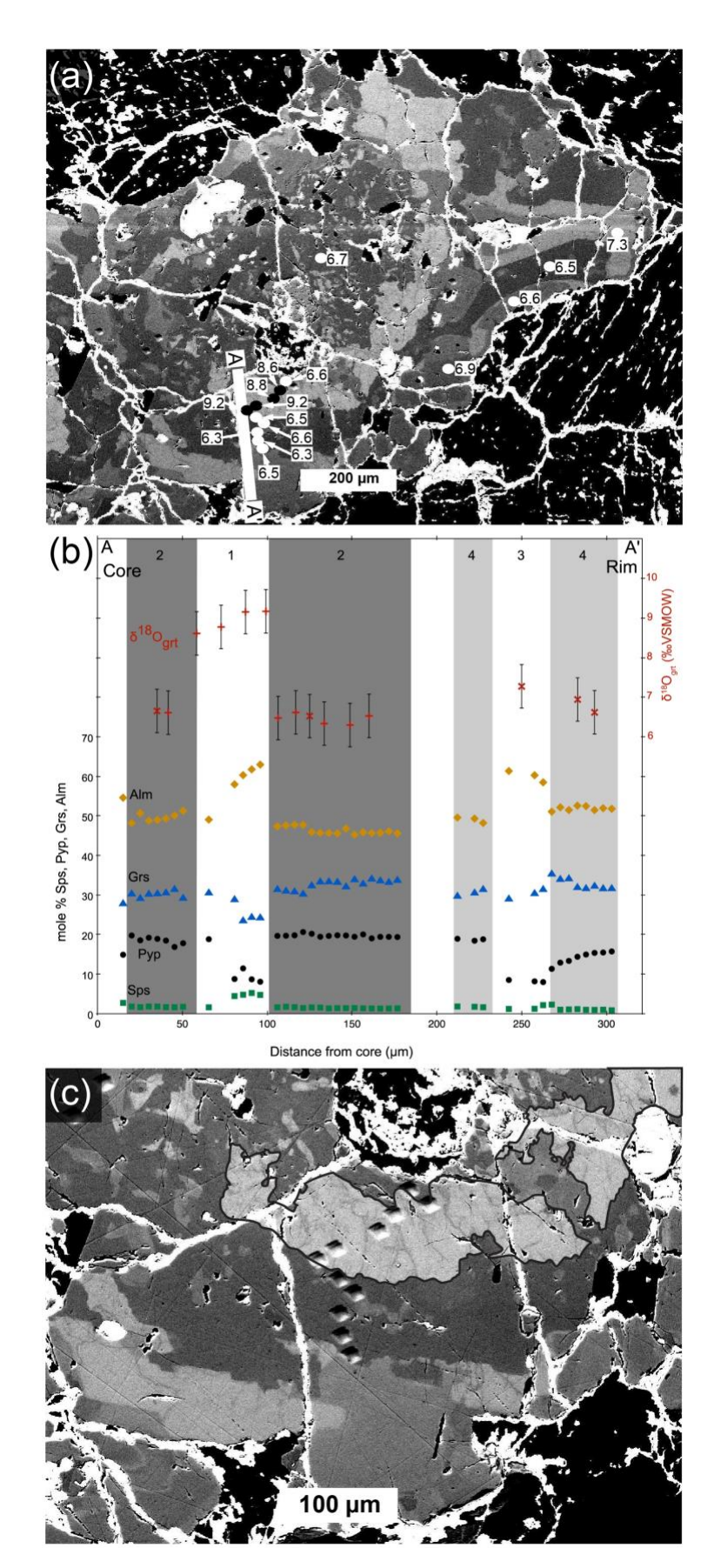


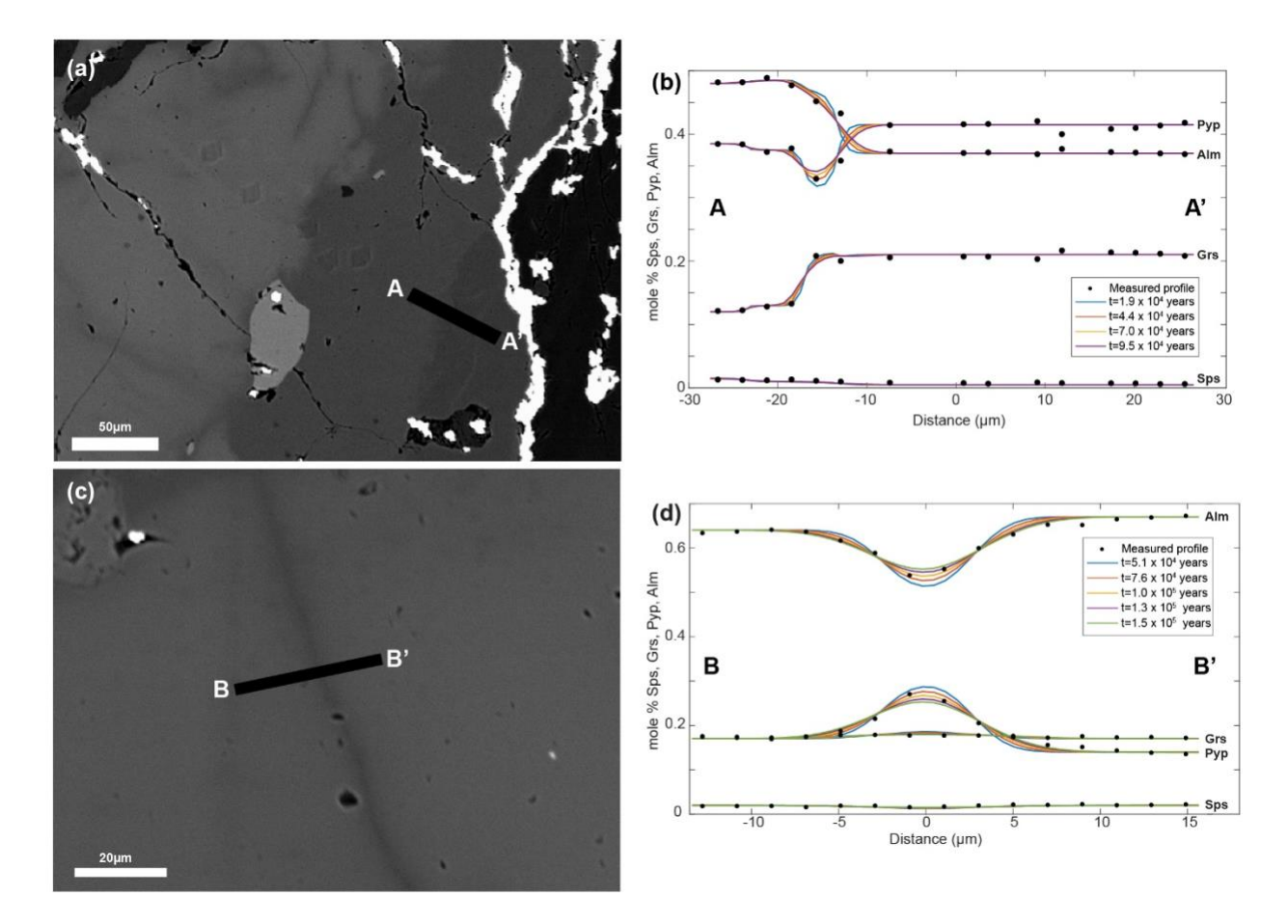












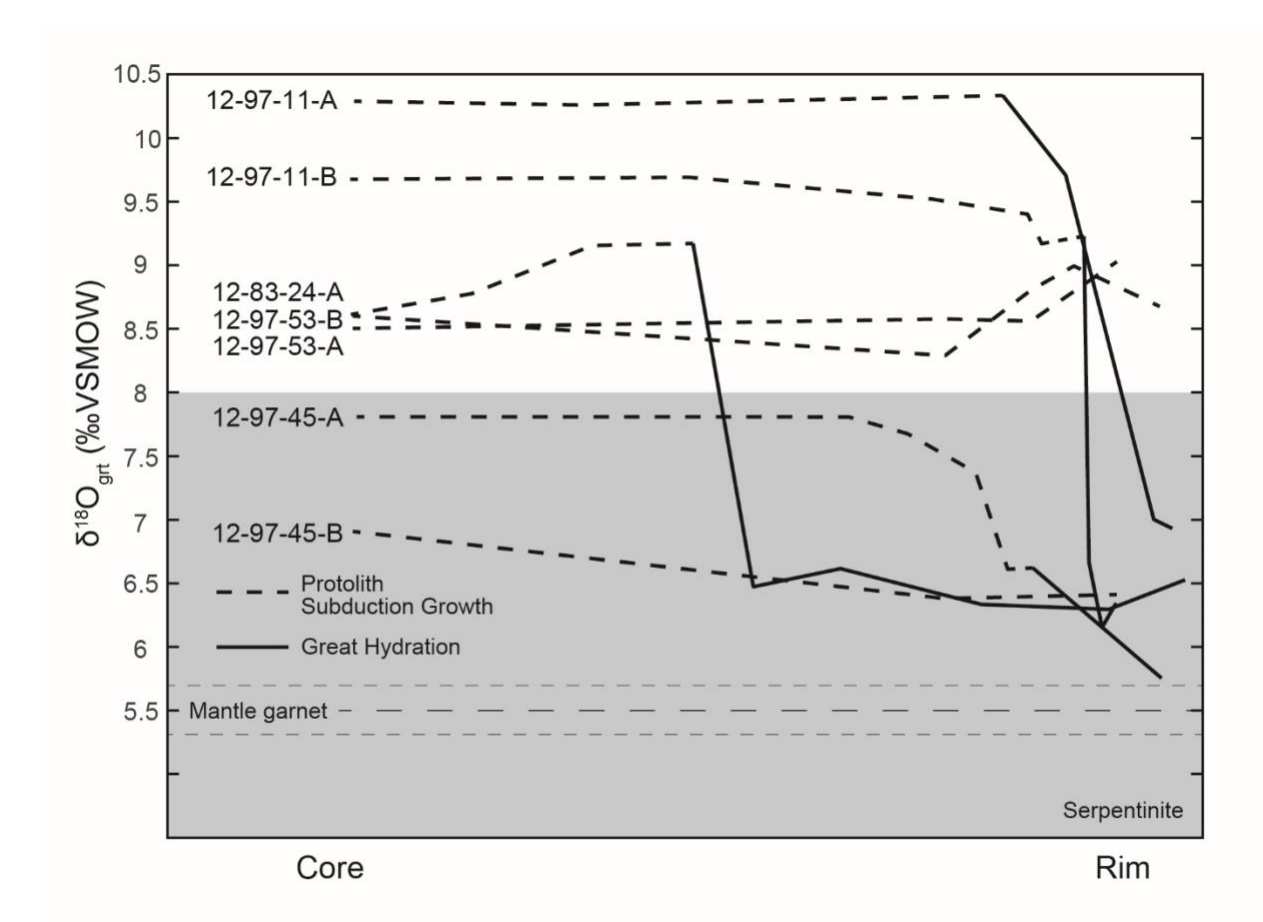


Table 1: Mineralogy and textural descriptions of the Moses Rock eclogite xenoliths

| Sample | Mineralogy | Garnet shape | BSE texture | Cation zoning | δ ¹⁸ O zoning (core-rim) |
|----------|---|------------------------|---|------------------|--|
| 12-97-11 | garnet+omphacite+zoisite±rutile±muscovite | subhedral | subhedral- concentric; healed fracturing | prograde | high to low |
| 12-97-45 | garnet+omphacite±zoisite±rutile | subhedral | subhedral- concentric; healed fracturing | prograde | high to low, and homogenous low |
| 12-97-53 | garnet+omphacite+zoisite±rutile | subhedral | subhedral- concentric; healed fracturing | prograde | homogenous high |
| 12-83-24 | garnet+omphacite±rutile±apatite | anhedral aggregates | non-concentric; healed fracturing; remnant atoll | atoll | high atoll, low core and rim |

Table 2: Representative major element and oxygen isotopes analyses from Moses Rock eclogite xenoliths

| Sample | 12-97-11 | | | | | | | | 12-97-45 | | | |
|-------------------|----------|------------------|--------|--------|--------|-----------------|------------------|--------|----------|-----------------|------------------|--------|
| Garnet | Α | | | | В | | | | Α | | | |
| | Core | Inter mediate | High-Z | Rim | Core | Healed Frac. | Inter mediate | Rim | Core | Healed Frac. | Inter mediate | Rim |
| SiO_2 | 38.14 | 38.91 | 38.23 | 37.71 | 37.36 | 38.54 | 38.54 | 39.32 | 36.72 | 38.96 | 39.26 | 39.84 |
| TiO ₂ | 0.009 | n/d | n/d | 0.092 | 0.128 | 0.022 | 0.050 | 0.128 | 0.028 | 0.069 | n/d | n/d |
| Al_2O_3 | 20.32 | 20.98 | 20.94 | 23.24 | 20.74 | 20.58 | 20.92 | 21.03 | 21.17 | 21.38 | 23.07 | 23.28 |
| Cr_2O_3 | 0.032 | 0.039 | 0.047 | 0.055 | 0.045 | 0.024 | 0.028 | 0.081 | 0.048 | 0.018 | 0.046 | 0.021 |
| FeO | 31.36 | 29.39 | 30.08 | 25.35 | 27.00 | 29.72 | 29.65 | 27.77 | 31.20 | 25.33 | 23.08 | 19.27 |
| MnO | 2.28 | 0.52 | 1.40 | 0.59 | 5.81 | 1.41 | 1.31 | 0.67 | 2.65 | 1.02 | 0.54 | 0.37 |
| MgO | 3.07 | 5.76 | 3.39 | 7.49 | 1.95 | 4.30 | 3.38 | 6.68 | 2.62 | 7.51 | 10.59 | 11.39 |
| CaO | 5.86 | 5.26 | 7.24 | 5.67 | 7.38 | 6.21 | 7.07 | 5.30 | 6.76 | 6.93 | 4.40 | 7.11 |
| Na₂O | n/d | 800.0 | 0.033 | 0.063 | 0.003 | 0.010 | 0.046 | 0.055 | 0.017 | 0.052 | 0.043 | 0.020 |
| Total | 101.06 | 100.87 | 101.36 | 100.26 | 100.41 | 100.83 | 100.99 | 101.04 | 101.20 | 101.26 | 101.03 | 101.30 |
| Si | 3.02 | 3.02 | 2.99 | 2.89 | 2.98 | 3.02 | 3.03 | 3.03 | 2.90 | 2.97 | 2.94 | 2.94 |
| Ti | 0.001 | 0.000 | 0.000 | 0.005 | 0.008 | 0.001 | 0.003 | 0.007 | 0.002 | 0.004 | 0.000 | 0.000 |
| Al | 1.89 | 1.92 | 1.93 | 2.10 | 1.95 | 1.90 | 1.94 | 1.91 | 1.97 | 1.92 | 2.04 | 2.03 |
| Cr | 0.002 | 0.002 | 0.003 | 0.003 | 0.003 | 0.001 | 0.002 | 0.005 | 0.003 | 0.001 | 0.003 | 0.001 |
| Fe ²⁺ | 2.07 | 1.91 | 1.97 | 1.63 | 1.80 | 1.95 | 1.95 | 1.79 | 2.06 | 1.61 | 1.45 | 1.19 |
| Mn | 0.15 | 0.03 | 0.09 | 0.04 | 0.39 | 0.09 | 0.09 | 0.04 | 0.18 | 0.07 | 0.03 | 0.02 |
| Mg | 0.36 | 0.67 | 0.40 | 0.86 | 0.23 | 0.50 | 0.40 | 0.77 | 0.31 | 0.85 | 1.18 | 1.25 |
| Ca | 0.50 | 0.44 | 0.61 | 0.47 | 0.63 | 0.52 | 0.60 | 0.44 | 0.57 | 0.57 | 0.35 | 0.56 |
| Na | 0.000 | 0.001 | 0.005 | 0.009 | 0.000 | 0.001 | 0.007 | 0.008 | 0.003 | 0.008 | 0.006 | 0.003 |
| XAlm | 67.23 | 62.64 | 64.26 | 54.44 | 58.92 | 63.55 | 64.37 | 58.91 | 66.10 | 52.09 | 47.94 | 39.29 |
| XPyp | 11.73 | 21.88 | 12.89 | 28.68 | 7.60 | 16.40 | 13.09 | 25.24 | 9.88 | 27.53 | 39.21 | 41.39 |
| XGrs | 16.09 | 14.37 | 19.83 | 15.60 | 20.63 | 17.00 | 19.68 | 14.41 | 18.34 | 18.26 | 11.71 | 18.57 |
| XSps | 4.95 | 1.11 | 3.02 | 1.28 | 12.85 | 3.06 | 2.87 | 1.43 | 5.68 | 2.12 | 1.15 | 0.76 |
| Mg# | 0.15 | 0.26 | 0.17 | 0.35 | 0.11 | 0.21 | 0.17 | 0.30 | 0.13 | 0.35 | 0.45 | 0.51 |
| δ ¹⁸ Ο | 10.29 | 10.33 | 9.71 | 6.93 | 9.68 | - | 9.40 | 6.34 | 7.80 | - | 6.62 | 5.75 |
| 2SD | ±0.65 | ±0.65 | ±0.65 | ±0.65 | ±0.56 | - | ±0.56 | ±0.56 | ±0.56 | - | ±0.56 | ±0.56 |

Table 2 cont'd

| 12-97-45 | | | 12-97-53 | | | | | | 12-83-24 | | | |
|----------|----------------|--------|----------|------------------|--------|--------|------------------|--------|----------|--------|--------|--------|
| В | | | Α | | | В | | | Α | | | |
| Core | Healed Frac | Rim | Core | Interme diate | Rim | Core | Interme diate | Rim | Core | Atoll | Rim 1 | Rim 2 |
| 37.21 | 39.10 | 39.05 | 37.91 | 37.72 | 38.03 | 37.95 | 37.60 | 38.25 | 38.96 | 37.66 | 38.13 | 37.72 |
| 0.111 | 0.032 | n/d | 0.148 | 0.156 | 0.090 | 0.185 | 0.239 | 0.006 | n/d | 0.077 | n/d | 0.008 |
| 21.49 | 21.81 | 23.18 | 20.64 | 20.53 | 21.36 | 20.65 | 20.79 | 21.10 | 21.52 | 20.49 | 22.10 | 21.33 |
| 0.049 | 0.041 | 0.055 | 0.014 | 0.031 | 0.056 | 0.022 | 0.031 | 0.041 | n/d | 0.031 | 0.035 | n/d |
| 31.27 | 25.92 | 23.91 | 30.38 | 32.59 | 30.25 | 30.86 | 32.91 | 30.76 | 22.57 | 28.92 | 22.05 | 29.15 |
| 1.09 | 0.72 | 0.66 | 1.39 | 0.46 | 0.95 | 1.74 | 1.48 | 1.24 | 0.73 | 2.42 | 0.61 | 0.28 |
| 3.59 | 7.30 | 10.34 | 2.60 | 2.04 | 2.90 | 2.52 | 2.17 | 2.93 | 5.21 | 2.28 | 5.16 | 2.56 |
| 6.10 | 6.66 | 4.01 | 7.36 | 6.90 | 7.94 | 7.06 | 5.91 | 6.83 | 11.76 | 8.91 | 12.84 | 9.63 |
| n/d | 0.030 | n/d | 0.018 | 0.011 | n/d | 0.146 | 0.116 | n/d | 0.034 | 0.027 | 0.018 | n/d |
| 100.90 | 101.62 | 101.21 | 100.46 | 100.44 | 101.57 | 101.14 | 101.25 | 101.16 | 100.78 | 100.81 | 100.95 | 100.67 |
| 2.93 | 2.97 | 2.93 | 3.01 | 3.01 | 2.98 | 3.00 | 2.98 | 3.01 | 2.99 | 2.98 | 2.92 | 2.97 |
| 0.007 | 0.002 | 0.000 | 0.009 | 0.009 | 0.005 | 0.011 | 0.014 | 0.000 | 0.000 | 0.005 | 0.000 | 0.000 |
| 1.99 | 1.95 | 2.05 | 1.93 | 1.93 | 1.97 | 1.92 | 1.94 | 1.96 | 1.95 | 1.91 | 1.99 | 1.98 |
| 0.003 | 0.002 | 0.003 | 0.001 | 0.002 | 0.003 | 0.001 | 0.002 | 0.003 | 0.000 | 0.002 | 0.002 | 0.000 |
| 2.06 | 1.65 | 1.50 | 2.02 | 2.18 | 1.98 | 2.04 | 2.18 | 2.03 | 1.45 | 1.91 | 1.41 | 1.92 |
| 0.07 | 0.05 | 0.04 | 0.09 | 0.03 | 0.06 | 0.12 | 0.10 | 0.08 | 0.05 | 0.16 | 0.04 | 0.02 |
| 0.42 | 0.83 | 1.16 | 0.31 | 0.24 | 0.34 | 0.30 | 0.26 | 0.34 | 0.60 | 0.27 | 0.59 | 0.30 |
| 0.51 | 0.54 | 0.32 | 0.63 | 0.59 | 0.67 | 0.60 | 0.50 | 0.58 | 0.97 | 0.75 | 1.05 | 0.81 |
| 0.000 | 0.004 | 0.000 | 0.003 | 0.002 | 0.000 | 0.022 | 0.018 | 0.000 | 0.005 | 0.004 | 0.003 | 0.000 |
| 67.11 | 53.78 | 49.66 | 66.26 | 71.56 | 64.99 | 66.84 | 71.78 | 66.88 | 47.36 | 61.75 | 45.65 | 62.91 |
| 13.75 | 27.00 | 38.28 | 10.12 | 7.99 | 11.09 | 9.75 | 8.45 | 11.35 | 19.49 | 8.67 | 19.02 | 9.85 |
| 16.78 | 17.70 | 10.67 | 20.56 | 19.42 | 21.86 | 19.60 | 16.51 | 19.03 | 31.61 | 24.36 | 34.06 | 26.64 |
| 2.36 | 1.52 | 1.38 | 3.06 | 1.03 | 2.06 | 3.81 | 3.26 | 2.74 | 1.54 | 5.23 | 1.28 | 0.60 |
| 0.17 | 0.33 | 0.44 | 0.13 | 0.10 | 0.15 | 0.13 | 0.11 | 0.15 | 0.29 | 0.12 | 0.29 | 0.14 |
| 6.91 | - | 6.41 | 8.50 | 8.58 | 9.03 | 8.60 | 8.29 | 8.68 | 6.65 | 9.16 | 6.30 | 7.27 |
| ±0.56 | - | ±0.56 | ±0.80 | ±0.80 | ±0.80 | ±0.80 | ±0.80 | ±0.80 | ±0.55 | ±0.55 | ±0.55 | ±0.55 |

Table 3: Results of multi-component garnet diffusion model

| Sample | Garnet | Traverse | Duration (years) 515°C 680°C | | | | | |
|----------|--------|-------------|------------------------------|-----------------------|-----------------------|-----------------------|--|--|
| | | | min | max | min | max | | |
| 12-97-11 | В | rim | 3.2 x 10 ⁵ | 3.2 x 10 ⁶ | 3.2 x10 ² | 3.2 x 10 ³ | | |
| 12-97-11 | В | fracture | 3.2 x 10 ⁶ | 3.2 x 10 ⁷ | 3.2 x 10 ³ | 3.2 x 10 ⁴ | | |
| 12-97-45 | Α | fracture | 1.0 x 10 ⁶ | 2.3 x 10 ⁸ | 1.9 x 10 ⁵ | 5.7 x 10 ⁵ | | |
| 12-97-45 | Α | inside rim | 5.1 x 10 ⁷ | 2.0 x 10 ⁸ | 2.5 x 10 ⁴ | 1.3 x 10 ⁵ | | |
| 12-97-45 | Α | outside rim | 1.8 x 10 ⁸ | 4.8 x 10 ⁸ | 1.9 x 10 ⁴ | 9.5 x 10 ⁴ | | |
| 12-97-45 | В | fracture | 2.5 x 10 ⁷ | 1.0 x 10 ⁸ | 5.1 x 10 ⁴ | 1.5 x 10⁵ | | |
| 12-97-53 | Α | core-to-rim | 3.8 x 10 ⁸ | 1.4 x 10 ⁹ | 4.1 x 10 ⁵ | 2.0 x 10 ⁶ | | |

Massive fluid influx beneath the Colorado Plateau

(USA) related to slab removal and diatreme

emplacement: Evidence from oxygen isotope zoning in

eclogite xenoliths

Hoover, William F.^{1,*}, Department of Geology, Oberlin College, Oberlin, OH, 44074, USA

Page, F. Zeb, Department of Geology, Oberlin College, Oberlin, OH, 44074, USA

Schulze, Daniel J., Department of Chemical and Physical Sciences, University of Toronto,

Mississauga, Ontario L5L 1C61, Canada

Kitajima, Kouki, WiscSIMS, Department of Geoscience, University of Wisconsin, Madison, WI 53706-1692, USA

Valley, John W., WiscSIMS, Department of Geoscience, University of Wisconsin, Madison, WI 53706-1692, USA

¹Present Address: Department of Geology, University of Maryland, College Park, MD 20742,

USA

*Corresponding author: whoover@umd.edu, +1 717 462 0055

Running title: Isotopic zoning in Colorado Plateau garnets

Final Publication:

Hoover WF, Page FZ, Schulze DJ, Kitajima K, Valley JW (2020) Massive fluid influx beneath the Colorado Plateau (USA) related to slab removal and diatreme emplacement: Evidence from oxygen isotope zoning in eclogite xenoliths. J. Petrol., 18p, doi: 10.1093/petrology/egaa102.

ABSTRACT

The Colorado Plateau has undergone as much as 1.8km of uplift over the past 80Ma, but never underwent the pervasive deformation common in the neighboring tectonic provinces of the western USA. To understand the source, timing and distribution of mantle hydration, and its role in plateau uplift, garnets from four eclogite xenoliths of the Moses Rock diatreme (Navajo Volcanic Field, Utah, USA) were analyzed in situ for δ^{18} O by secondary ion mass spectrometry. These garnets have the largest reported intra-crystalline oxygen isotope zoning to date in mantlederived xenoliths with core-to-rim variations of as much as 3%. All samples have core δ^{18} O values greater than that of the pristine mantle ($\sim 5.3\%$, mantle garnet as derived from mantle zircon; Valley et al., 1998; Page et al., 2007) consistent with an altered upper oceanic crust protolith. Oxygen isotope ratios decrease from core to rim recording interaction with a low- δ^{18} O fluid at high temperature, likely derived from serpentinite in the foundering Farallon slab. All zoned samples converge at a δ^{18} O value of ~6%, regardless of core composition, suggesting that fluid infiltration was widely distributed. Constraints on the timing of this fluid influx, relative to diatreme emplacement, can be gained from diffusion modeling of major element zoning in garnet. Modeling using best-estimates of peak metamorphic conditions (620°C, 3.7GPa) yield durations of <200 thousand years suggesting that fluid influx and diatreme emplacement were temporally linked. These eclogite xenoliths from the Colorado Plateau record extensive fluid influx pointing to complex hydration-dehydration processes related to flat-slab subduction and foundering of the Farallon plate. Extensive hydration of the lithospheric mantle during this fluid influx may have contributed to buoyancy driven uplift of the Colorado Plateau and melt-free emplacement of Navajo Volcanic Field diatremes.

Keywords: eclogite; oxygen isotopes; SIMS; xenolith; garnet; Colorado Plateau

INTRODUCTION

Recent work has suggested that the uplift of the Colorado Plateau and other undeformed continental regions in the western USA was driven, at least in part, by the buoyancy of a hydrated lithosphere (e.g., Humphreys et al., 2003; Jones et al., 2015; Schulze et al., 2015). Abundant evidence for this hydration can be found in the hydrated mantle xenoliths of the Navajo Volcanic Field. Schulze et al. (2015) presented geochronologic evidence in eclogite xenoliths for a widespread fluid influx beneath the Colorado Plateau at ~28Ma calling this event the "Great Hydration" and arguing that this fluid pulse could have serpentinized a significant portion of the underlying plateau lithosphere. If uplift was driven by such a widespread "Great Hydration" then we could expect to find further geochemical evidence of this fluid pulse in these and other xenoliths. This could provide information about the source, composition, distribution and timing of the fluid infiltration, and its tectonic framework. While a number of previous studies have focused on establishing the age and pressure-temperature conditions of the various xenoliths, evidence for mantle metasomatism, and the generation of unusual lithologies (e.g., Smith & Griffin, 2005; Smith, 2010; Schulze et al., 2014), only a single study has focused on the source of the infiltrating fluid(s) (Marshall et al., 2017), and the timing and relationship to diatreme emplacement remain largely unconstrained. To study the source, timing and distribution of fluid beneath the Colorado Plateau during uplift, four eclogite xenoliths were selected for in situ oxygen isotope analysis and diffusion modeling of major element zoning in garnet. These xenoliths are thought to have been tectonically eroded, transported and underplated beneath the Colorado Plateau by the shallowly subducting Farallon slab, making them a potential record of the subduction-related hydration of the sub-plateau lithospheric mantle (Smith, 2010, 2013).

In situ analysis of oxygen isotope ratios in garnet has been particularly successful in identifying and differentiating fluid sources in eclogites (e.g., Russell *et al.*, 2013; Errico *et al.*,

2013; Page *et al.*, 2014; Rubatto & Angiboust, 2015). Previous bulk measurements of oxygen isotope compositions of xenoliths from the Colorado Plateau and neighboring Rio Grande Rift preserve evidence of interaction with subducted material (Smith, 1995; Smith *et al.*, 2004; Perkins *et al.*, 2006; Marshall *et al.*, 2017), but improvements in microanalytical techniques offer the possibility of accessing a more detailed fluid history recorded in intra-mineral isotopic zoning (e.g., Kita *et al.*, 2009; Valley & Kita, 2009; Page *et al.*, 2010; Ickert & Stern, 2013). Concentric zoning records sequential snapshots of the mineral growth environment, placing isotopic compositions in a relative chronology, and illuminating evolving or abruptly changing fluid compositions.

The timing of transient processes (e.g., fluid infiltration) can be constrained at very short timescales (<1Myr) and directly connected to chemical information preserved in zoning by examining diffusion profiles of major elements in garnet (e.g., Jollands et al., 2018; Broadwell et al., 2019). The eclogite xenoliths from the Navajo Volcanic Field of the Colorado Plateau are particularly well-suited for this method as they are notable for their low temperatures of formation (e.g., Usui et al., 2003; Hernández-Uribe & Palin, 2019). At these temperatures, intracrystalline diffusive length-scales are small relative to zone widths, meaning zoning can generally be expected to survive through peak metamorphism and exhumation for reasonable residence times (e.g., Vielzeuf *et al.*, 2005a; Page *et al.*, 2010; 2014). Preserved diffusion profiles can be modeled to calculate the timing of garnet growth relative to diatreme emplacement. In this study, we use secondary ion mass spectrometry (SIMS) to analyze oxygen isotope ratios *in situ* at the ~10μm scale in garnet and couple these measurements with diffusion modeling of divalent cations to understand the source, timing and distribution of fluid infiltration in the Colorado Plateau lithospheric mantle.

GEOLOGIC SETTING

The four eclogite xenoliths analyzed in this study are all from the Moses Rock diatreme, part of the Navajo Volcanic Field, in the Colorado Plateau (Fig. 1). The Colorado Plateau has been uplifted ~1.8km over the last 80Ma, however, the temporal distribution of this uplift is poorly understood (e.g., Sahagian *et al.*, 2002; Flowers *et al.*, 2008; Liu & Gurnis, 2010). While the plateau was uplifted, its interior remained relatively undeformed during the Sevier-Laramide orogeny and Basin and Range extension responsible for the extensive deformation of the neighboring Rio Grande Rift, Rocky Mountains and Basin and Range tectonic provinces (e.g., McGetchin *et al.*, 1977; Humphreys *et al.*, 2003; Flowers *et al.*, 2008; Liu & Gurnis, 2010). During a portion of the 80Ma period of uplift, the Farallon slab was shallowly subducting beneath the plateau resulting in eastward migration of arc volcanism and hydration of the overlying lithosphere by fluids released by the slab during dehydration (e.g., Dickinson & Snyder, 1978; Lipman, 1992; Smith *et al.*, 1999; Saleeby, 2003; Dickinson, 2004).

The Navajo Volcanic Field (NVF) is at the center of the Colorado Plateau and comprises potassic mafic minettes and serpentinite diatremes emplaced between 19 and 32Ma (Fig. 1; e.g., Naeser, 1971; Helmstaedt & Doig, 1975; Roden *et al.*, 1979; Laughlin *et al.*, 1986; Nowell, 1993; Smith *et al.*, 2004), concurrent with interpreted slab removal between ~20 and 40Ma (e.g., Coney & Reynolds, 1977; Humphreys, 1995; Humphreys *et al.*, 2003; Humphreys, 2009; Levander *et al.*, 2011; Cather *et al.*, 2008). The diatremes are composed of serpentinized ultramafic microbreccia (SUM), and were emplaced without a melt component as SUM-gas mixtures (McGetchin & Silver, 1970, 1972; Naeser, 1971; Roden *et al.*, 1979; Roden, 1981). In addition to the SUM matrix, these diatremes contain crustal fragments sampled along the emplacement path and minor (<1%) quantities of mantle xenoliths and xenocrysts (McGetchin & Silver, 1970; 1972; Roden, 1981). These mantle-derived materials include discrete grains of pyrope, diopside

and forsterite, and xenoliths of garnet and spinel peridotites, pyroxenites, garnetites and eclogites, many of which show textural and chemical evidence of extensive fluid-rock interaction (e.g., McGetchin *et al.*, 1977; Helmstaedt & Schulze, 1988, 1991; Smith *et al.*, 2004; Smith & Griffin, 2005; Smith, 2013; Schulze *et al.*, 2014).

While the catalyst for diatreme emplacement is still unclear, Smith (2010) identified evidence in peridotite xenoliths for a short-lived (hundreds of years) thermal pulse that must have occurred immediately prior to diatreme emplacement. He attributed this thermal pulse to minette intrusion which triggered massive devolatilization of hydrated mantle and diatreme emplacement (Smith & Levy, 1976; Smith, 2010). Preexisting structural weaknesses may have played a role in diatreme emplacement as well, since diatremes are spatially associated with monoclines inferred to be reactivated Proterozoic shear zones (McGetchin et al., 1977; Davis & Bump, 2009; Smith, 2010). Current estimates for the pressure and temperature of the diatreme source based on thermobarometry of xenoliths and discrete mineral grains suggest pressures greater than 2.4GPa and temperatures of at least 470°C (e.g., Smith, 2010, 2013; Schulze et al., 2015). These conditions are consistent with recent peak pressure-temperature (P-T) estimates for eclogite xenoliths of 620°C and 3.7GPa from thermodynamic modeling (Hernández-Uribe & Palin, 2019), and with previous estimates from garnet-clinopyroxene-phengite thermobarometry (Helmstaedt & Schulze, 1988; Usui et al., 2003; Smith et al., 2004; Schulze et al., 2015; Hernández-Uribe & Palin, 2019) and the presence of coesite and lawsonite (e.g., Helmstaedt & Doig, 1975; Smith & Zientek, 1979; Usui et al., 2003).

The age and protolith of the eclogite xenoliths from these diatremes have been the subject of some controversy (e.g., Helmstaedt & Doig, 1975; Smith & Zientek, 1979; Wendlandt *et al.*, 1993; Usui *et al.*, 2003; Smith *et al.*, 2003). Ages of 21 to 33Ma from Sm-Nd and U-Pb dating of mineral separates and *in situ* U-Pb dating of zircons and Th-Pb dating of monazite are consistent

with the timing of diatreme emplacement (Wendlandt *et al.*, 1996; Smith *et al.*, 2004; Usui *et al.*, 2003; Schulze *et al.*, 2015). Thermal ionization mass spectrometry and SIMS U-Pb dating of zircon also yielded a range of ages from 81Ma to diatreme emplacement interpreted to record recrystallization during prograde metamorphism (Smith *et al.*, 2004; Usui *et al.*, 2006; Malik *et al.*, 2017). However, some xenoliths contain a discordant zircon population that yield Mid-Proterozoic ages (~1.5 to 1.7Ga; Smith *et al.*, 2004; Malik *et al.*, 2017) similar to the Nd model ages of Wendlandt *et al.* (1993). While it was originally thought that these eclogites were genetically related to eclogites in the Franciscan Complex, California (e.g., Helmstaedt & Doig, 1975), the Mid-Proterozoic ages are far older than the initiation of Farallon subduction (Mulcahy *et al.*, 2018) and require a source within the North American lithosphere (Smith *et al.*, 2004). Based upon prograde garnet zoning and these age constraints, the current model for these eclogites invokes tectonic erosion from the forearc lithosphere near the trench and transportation along the subduction interface to the diatreme source region (e.g., Helmstaedt & Schulze, 1991; Smith, 2010; Schulze *et al.*, 2015).

SAMPLE DESCRIPTION

Petrography

Four eclogite xenoliths were chosen for this study, and can be broadly separated into two groups: the three samples with the 12-97 prefix (12-97-11, 12-97-45, and 12-97-53), and the texturally different sample 12-83-24 (Fig. 2). All samples are dominated by omphacite and garnet and contain accessory rutile and opaque minerals. Zoisite is found only in the 12-97 samples and occurs as tabular aggregates or layers of acicular crystals. These aggregates have been interpreted as lawsonite pseudomorphs because of their tabular shape, chemical composition and the presence of relict lawsonite cores in some samples (Helmstaedt & Doig, 1975; Smith & Zientek,

1979; Usui *et al.*, 2003; Usui *et al.*, 2006). Where present, foliation is defined by zoisite layers. In the 12-97 samples, garnet is porphyroblastic and shows a wide range in abundance (~5-40%) and size (0.2mm to 3mm) between and within individual samples. Rare atoll garnet textures with omphacite cores are found in some of the 12-97 samples (Fig. 3a and b); while atoll garnet textures in 12-83-24 are overgrown by new garnet (Fig. 3c). Mineralogically, Sample 12-83-24 is distinguished by the absence of zoisite and the presence of significant accessory apatite. Garnet in sample 12-83-24 occurs as laterally extensive layers up to 3mm wide with individual porphyroblasts indistinguishable in plane or cross-polarized light. These garnet aggregates define a moderate foliation.

Garnet Textures

For all samples, letters following sample numbers are used to differentiate individual garnets within that sample as opposed to the sample in general. High-contrast back-scattered electron (BSE) images of garnet porphyroblasts from the 12-97 samples show irregular concentric zoning with subhedral to anhedral zone boundaries throughout (Table 1; Figs. 4-6). Garnet rims are heavily embayed, such that intermediate and rim zones are discontinuous in some samples (e.g., Fig. 4b and 5a). Average atomic number (*Z*) generally decreases from core to rim in the 12-97 samples, though mottling and incomplete low- and high-*Z* zones disrupt this general decrease in some garnets (e.g., 12-97-11-A, Fig. 4a). Linear features visible in BSE crosscutting core zones are present in all of the samples in this study and are interpreted as fractures healed by later garnet growth (e.g., Fig. 4b, 5b, 6a and 7c).

As noted above, sample 12-83-24 is mineralogically and texturally distinct from the other samples in this study (Table 1; Fig. 2b and 7a). BSE images of garnet aggregate layers from this sample exhibit extremely complex patchwork zoning. This style of non-concentric zoning has

been reported in other settings and attributed to transport-limited growth or overgrowth zoning (e.g., Yang & Rivers, 2001; Angiboust *et al.*, 2014). In garnet 12-83-24-A, the only indication of a core-rim relationship is the incomplete subhedral highest-*Z* zone that appears to be a remnant of concentric zoning. This highest-*Z* zone is found with a similar ring-like morphology in other garnets from this sample with some preserved euhedral faces (Fig. 3c). This remnant ring zone in all cases is overgrown (both in the core and rim) by multiple anhedral, non-concentric and discontinuous zones. Healed fractures are found in the two highest-*Z* zones in this garnet.

ANALYTICAL METHODS

All samples were analyzed as polished thin sections. The JEOL JSM-5610 LV scanning electron microscope (SEM) at Oberlin College was used to collect BSE images to guide ion probe analyses and secondary electron (SE) images to characterize ion probe pits post-analysis.

The CAMECA IMS 1280 ion microprobe at the WiscSIMS lab at the University of Wisconsin-Madison was used to analyze oxygen isotopes. Thin sections were prepared for analysis by cutting and grinding into 2.54cm circular sections. Garnets selected for analysis were located within ~5mm of the center of the section. After garnets were selected for analysis, UWG-2 garnet standard (Valley *et al.*, 1995) was embedded near the center of each section using epoxy and polished until coplanar with the sample. Thin section disks were gold coated before analysis. Oxygen isotope ratios were measured using the methods of Kita *et al.* (2009) and Valley & Kita (2009), with a focused beam of Cs⁺ ions at a current of 1.8-2.2 nA and a spot size of ~12μm. Brackets of eight UWG-2 standard analyses were used to correct intermediate unknowns for instrumental mass fractionation (not including bias due to different garnet cation compositions). The reproducibility of the UWG-2 standard for each bracket was assigned as the precision for intervening sample analyses, this reproducibility is a more conservative estimate of precision than

the internal errors (typically 0.2% 2S.E.) based on counting statistics (Kita *et al.*, 2009). The instrumental precision based on UWG-2 reproducibility ranged from $\pm 0.23\%$ to $\pm 0.62\%$ (2S.D.) with the majority of brackets falling close to the lower value (Electronic Appendix 1,2). 16 OH/ 16 O was measured during each analysis in order to monitor for inclusions or garnet domains containing a hydrogrossular component (e.g., Wang et al., 2014). All samples have similar values of 16 OH/ 16 O to the UWG-2 garnet standard, indicating similarly low OH content.

Oxygen isotope analysis of garnet by SIMS is strongly dependent on cation chemistry. Vielzeuf *et al.* (2005b) found that in garnet low in ferric iron, instrumental bias in measured oxygen isotope ratios is predominantly controlled by grossular content. The method of Page *et al.* (2010) was used to correct for the effect of compositional bias during ion microbe analysis. Analyses of oxygen isotope ratios of eight garnet standards that bracket the sample compositions (UWG-2, AlmSE, SpsSE, PypDM, GrsSE, Bal509, 13-63-44 and R-53) were carried out during the same analytical session and used to create a calibration curve relating bias with Ca content of garnets (Electronic Appendix 1, 2 and 3). Electron microprobe analyses of cation composition were taken next to each ion microprobe pit in unknown samples and compared to the calibration curve to determine the appropriate correction for cation composition. Grossular content ranged from 10-36%, resulting in a matrix correction of -0.3 to +1.0% relative to UWG-2. Uncertainty in the matrix correction was assumed to be 0.5% (2SD) and was combined in quadrature with instrumental precision from bracketing UWG-2 analyses for total uncertainties of ±0.55% to ±0.80% (2SD).

Major element analyses were carried out with the CAMECA SX100 electron microprobe at the University of Michigan, Ann Arbor. The gold coating for ion microprobe analysis was removed from the thin section disks, which were then carbon coated and analyzed using a 15kV, 10nA focused beam with a 20 second counting time. Natural and synthetic silicate and oxide

standards were used, and data were processed using a CAMECA phi-rho-Z-type correction with oxygen calculated by stoichiometry. Ferric iron was negligible when estimated using the method of Quinn et al. (2016). Post-analysis SE images of each ion microprobe pit were taken to ensure that pits were inclusion free. Electron microprobe points and SIMS pits that contained inclusions or intersected cracks were excluded from this study but are included in the Data Repository. Pits that fell on the boundary between two δ^{18} O zones were excluded or indicated as such.

RESULTS

Garnet oxygen isotope zoning

Garnets from the 12-97 samples can be separated into two groups based upon oxygen isotope zoning (Tables 1 and 2). Garnets 12-97-11-A, 12-97-11-B and 12-97-45-A are all zoned in $\delta^{18}O$ with elevated- $\delta^{18}O$ cores (10.1±0.5‰, 9.5±0.4‰ and 7.3±1.2‰, mean and 2SD, respectively) and lower- $\delta^{18}O$ rims (6.9±0.2‰, 6.3±0.5‰ and 5.8‰, mean and 2SD, respectively) (Figs. 4, 5a and c). Garnets 12-97-45-B, 12-97-53-A and 12-97-53-B are all comparatively homogeneous in oxygen isotope composition (Fig. 5b and 6). However, the $\delta^{18}O$ values in the garnets from 12-97-53 are higher than those in 12-97-45-B (8.7±0.5‰ compared to 6.6±0.6‰, mean and 2SD, respectively). In the garnet from sample 12-83-24, $\delta^{18}O$ values are bimodally distributed (Fig. 7). The incomplete subhedral high-*Z* zone has higher $\delta^{18}O$ values and the various core and rim patchwork zones have lower $\delta^{18}O$ values (8.9±0.6‰ and 6.6±0.6‰, mean and 2SD, respectively).

Garnet major element zoning

Garnets in the 12-97 samples have rims that are depleted in almandine (Alm) and enriched in pyrope (Pyp), relative to the cores. Grossular (Grs) varies little or inversely to Pyp. Traverses

normal to zone boundaries (step sizes ranging from \sim 1 to 3 μ m) show gradual changes in cation composition over \sim 10 to 25 μ m consistent with diffusive relaxation of an initially sharp boundary. In the garnets from samples 12-97-11 and 12-97-45, high-resolution (\sim 1 to 2 μ m step size) electron microprobe traverses of healed fractures show diffusive relaxation. The major element composition of these features is most similar in composition to the garnet in the next rim-ward zone suggesting they grew concurrently (e.g., Fig. 4b, 5a, Table 2).

As expected based upon garnet textures, cation zoning in garnet 12-83-24-A is highly variable (Table 2; Fig. 7b). Based upon major element data, four zones can be distinguished, corresponding to the four zones visible in the BSE image (Figs. 7a and 7c). Zone 1 shows distinctly lower Grs and higher Sps than the other three zones. Zones 2, 3 and 4 have similar Grs and Sps, but are distinct in Pyp and Alm.

DIFFUSION MODELING

Model setup

Traverses across zone boundaries in all 12-97 samples show small-scale gradients in major elements (<20µm in width), consistent with diffusive exchange. To estimate the timing of garnet growth relative to major tectonic events experienced by these eclogites, we created a numerical model in MATLAB to describe the diffusion of major divalent cations in garnet. This model was applied to zone boundaries and healed fractures in all 12-97 samples. Our model uses a finite difference approximation of the one-dimensional diffusion equation for a planar geometry and infinite reservoir boundary condition (Electronic Appendix 4; Crank, 1975). These conditions are justified because all traverses are short relative to garnet radii and located at a distance from grain boundaries several times the width of the diffusion profile (Fig. 8a and 8c). Fit of the modeled

and measured profiles was assessed visually (Fig. 8b and 8d). Initial single-step functions in concentration were assumed unless multiple initial step functions were necessary to reproduce the topology of measured profiles (Fig. 8b). Spatial resolution of the model was at least as fine as the measured major element traverses, and time steps varied from 1200 years to 6 million years to maintain the stability of the model. The diffusivities of divalent cations in garnets are heavily dependent on composition (e.g., Carlson, 2006; Ganguly, 2010), so tracer diffusivities varied spatially and were recalculated at each time step in response to diffusive changes in composition. Due to the mixed Alm-Pyp-Grs composition of these garnets, tracer diffusivities were calculated using the method of Carlson (2006), as these compositions are not well represented by experimental diffusion couples (e.g., Chakraborty & Ganguly, 1992; Ganguly *et al.*, 1998). Parameters used to calculate diffusivity (frequency factor, sensitivity to unit-cell dimension, activation energy, activation volume) were varied within uncertainties specified in Carlson (2006) as needed to maximize the fit of the model. This generally involved maximizing the diffusivity of Fe and minimizing that of Mg and Ca relative to Mn.

P-T-fO2 inputs

Peak temperatures and thermal histories of the NVF eclogite xenoliths represent the main source of uncertainty in our model. Hernández-Uribe & Palin (2019) used thermodynamic modeling of lawsonite-bearing eclogite xenoliths from Moses Rock to calculate peak conditions of 3.7GPa ± 0.1GPa and 620°C ± 50°C. These results using current thermodynamic modeling methods overlap within uncertainty all previous temperatures of Moses Rock eclogite xenoliths calculated from garnet-clinopyroxene-phengite thermobarometry (515 to 680°C; Smith *et al.*, 2004; Schulze *et al.*, 2015). If consideration is extended to garnet-clinopyroxene temperatures calculated using assumed pressures >2GPa for all NVF eclogite xenoliths, nearly all temperature estimates

overlap those from thermodynamic modeling within the uncertainty (Helmstaedt & Schulze, 1988; Usui *et al.*, 2003; Smith *et al.*, 2004; Schulze *et al.*, 2015; Hernández-Uribe & Palin, 2019). Based on the agreement between traditional mineral thermometry estimates and calculated temperatures from thermodynamic modeling, the most recent pressure and temperature estimates for Moses Rock eclogite xenoliths were utilized in our diffusion models accounting for the upper and lower uncertainty bounds (Hernández-Uribe & Palin, 2019).

Limited information is available regarding the metamorphic P-T path of the NVF eclogites or the timing of garnet rim growth and fracture healing. For this reason, we have chosen to model diffusion at a constant temperature, however, the impact of this uncertainty is minimal based on the following geodynamic and theoretical constraints. Prolonged cooling during exhumation can be ruled out as diatreme emplacement is interpreted to have been rapid (e.g., Smith & Roden, 1981). Likewise, post-peak, pre-emplacement cooling accommodated by changes in the subduction zone thermal structure are unlikely during stable flat slab subduction. Flat slab subduction occurs under limited thermo-mechanical conditions (thick or young oceanic crust) characterized by warm geothermal gradients (e.g., Syracuse *et al.*, 2010; Huangfu *et al.*, 2016). The maintenance of flat slab subduction until contemporaneous slab foundering and diatreme emplacement (e.g., Roden *et al.*, 1979; Cather *et al.*, 2008) suggests no changes in thermal structure occurred prior to slab foundering. These arguments suggest that no significant cooling (in the context of diffusion modeling) occurred post-garnet rim growth.

The effect of early garnet growth under cooler prograde conditions (heating path) cannot be ruled out but would have a minimal effect on our results. Diffusivity is exponentially dependent on temperature so diffusion distance will be dominated by the highest temperatures reached by these garnets (during peak metamorphism) even if they grew at significantly lower temperatures. In addition, the locations of our modeled chemical gradients near the rims of the

garnets suggests that they represent the later portions of garnet growth and thus near-peak temperatures. Though more uncertain than peak temperature estimates due to the challenge of establishing equilibrium relationships, garnet-clinopyroxene thermometry of garnet interiors from NVF eclogite xenoliths largely overlap our modeled temperatures (8 of 11 greater than 570°C). Based on this evidence, garnet rim growth significantly outside our modeled temperatures is unlikely, and would have a limited effect on our results.

The tracer diffusivity of divalent cations in garnet is dependent on the oxygen fugacity (fO₂), with variations of ~1.5 log units across a reasonable range of oxygen fugacities.

Unfortunately, fO₂ is difficult to assess in eclogites where buffering assemblages (e.g., fayalite-magnetite-quartz) are missing or redox-sensitive element partitioning is uncalibrated. An estimate for the oxygen fugacity of a minette and associated ultramafic breccia from the Buell Park pipe (NVF) yielded values close to the fayalite-magnetite-quartz buffer using spinel-ilmenite oxybarometry (Roden & Smith, 1982). While it is unclear how representative this is of diatreme sources across the NVF, it was used in our model in the absence of better estimates.

DISCUSSION

Oxygen isotope compositions of eclogite xenoliths

This study reports the largest intra-crystalline δ^{18} O variation reported in mantle-derived xenoliths with variations of up to ~3‰ from core to rim across some garnets. This is in contrast with previous studies which found little or no variation outside of uncertainty in eclogitic garnets from kimberlitic xenoliths. Russell *et al.* (2013) used SIMS to analyze garnet from several kimberlitic eclogite xenoliths and reported subtle variations of ~0.5‰ and ~1‰. However, variation was not systematic, and they concluded that their garnets were largely homogeneous in oxygen isotope composition, attributing this to diffusional resetting during long residence times at mantle

temperatures. Smit *et al.* (2014) analyzed garnet separates from kimberlitic eclogite xenoliths using SIMS, however they found no significant variation in δ^{18} O and reported their results as whole crystal averages. Most recently, Riches *et al.* (2016) used SIMS to assess the record of diamond-forming metasomatism in a kimberlite-sourced eclogite xenolith. They found their garnets to be homogeneous in oxygen isotope composition and concluded that, though eclogite xenoliths may retain their oceanic crust protolith signature for long periods of time in the mantle, δ^{18} O homogeneity in garnet is likely a general characteristic of mantle eclogites. Riches *et al.* suggested that metasomatic alteration of oxygen isotope signatures in eclogite during diamond formation was unlikely, as any fluids passing through the mantle would be buffered to mantle δ^{18} O values by the inherently low fluid-rock ratio. The results of this study contrast with those of Riches *et al.*, recording and preserving evidence of interaction with a lower- δ^{18} O reservoir. This suggests that in instances of low geothermal gradients, proximal and extensive fluid production or rapid removal from mantle conditions, oxygen isotope homogeneity should not be assumed.

As has been the case in many studies of eclogite mantle xenoliths (e.g., Russell *et al.*, 2013; Smit *et al.*, 2014; Radu *et al.*, 2019), the δ^{18} O values of the eclogite xenoliths in this study (Fig. 9; Table 2) range well beyond that of mantle garnet of 5.3±0.6‰ as derived from mantle zircon (Valley *et al.*, 1998; Page *et al.*, 2007). Oceanic basalt is elevated to δ^{18} O values above the pristine mantle by low-temperature alteration (e.g., Gregory & Taylor, 1981; Alt *et al.*, 1986; Eiler, 2001). This supports previous major element, Sr isotope and O isotope evidence for an oceanic crust protolith for the NVF eclogite xenoliths (e.g., Helmstaedt & Doig, 1975; Usui *et al.*, 2003; Smith *et al.*, 2004). Putlitz *et al.* (2000) found that subducted mafic rocks recrystallizing in a closed system will adopt the bulk-rock oxygen isotope signature of their protolith, supporting the interpretation that the elevated δ^{18} O values of the eclogite xenoliths in this study reflect their protolith. Oxygen isotopes also have a negligible amount (<0.2‰) of

temperature or pressure fractionation between garnet and the other minerals present in eclogite (Clayton *et al.*, 1975; Valley, 2003), so analyses of garnet in this study are expected to reflect the bulk- δ^{18} O of the eclogite. Based on this previous work, elevated δ^{18} O values in garnet cores from these eclogite xenoliths are interpreted to reflect the oxygen isotope signature of their altered upper oceanic crust protolith adopted during closed-system growth.

Fluid source inferred from garnet rims

The rims of some of the garnets in this study show significant differences in isotopic composition relative to their cores indicating a change in fluid composition as opposed to P-T conditions (Fig. 9). In garnets 12-97-11-A and -B and, to a lesser extent, 12-97-45-A, δ^{18} O values decrease sharply from cores to rim values approaching that of the pristine mantle (Figs. 4, 5a, 5c). Because the isotopic fractionation between eclogitic minerals is minimal at the pressures and temperatures of eclogite formation (Clayton *et al.*, 1975; Valley, 2003), the only way to decrease the δ^{18} O value of the garnet is by interaction with externally-derived fluids from a low- δ^{18} O reservoir at high temperatures.

In the context of these samples, there are several possible sources consistent with this low- δ^{18} O signature. Altered lower oceanic crust has δ^{18} O values lower than the mantle values but is generally the least hydrated portion of downgoing slab and thus has little fluid with which to infiltrate these eclogites (e.g., Cartwright & Barnicoat, 1999; Eiler, 2001; Hacker, 2008). This is also true of unaltered mantle wedge or slab mantle which has an appropriate δ^{18} O value (~5.3‰, mantle garnet derived from mantle zircon; Valley *et al.*, 1998; Page *et al.*, 2007), but is nominally anhydrous (Valley *et al.*, 1998; Page *et al.*, 2007). Serpentinite can have δ^{18} O values of ~1 to 8‰ (e.g., Cartwright & Barnicoat, 1999; Eiler, 2001; Früh-Green *et al.*, 2001; Miller *et al.*, 2001; Scambelluri *et al.*, 2004; Marshall *et al.*, 2017), and generally dehydrates at temperatures of

~600°C, consistent with the diatreme source region (e.g., Ulmer & Trommsdorff, 2009). A serpentinite source could be in the mantle wedge (hydrated by the Farallon slab) or in the downgoing slab (hydrated along faults on the ocean floor, e.g., Ranero *et al.*, 2003).

We consider a serpentinite-derived fluid to be the most likely source of the low- δ^{18} O rims for a number of reasons. Marshall et al. (2017) explained low- δ^{18} O fluids recorded in hydrated peridotite NVF xenoliths with a serpentinite-derived fluid source within the Farallon slab. Serpentine dehydration inferred from textures and compositions of zoned olivine in a Cr-dunite (former low-pressure serpentinite) xenolith from the Green Knobs diatreme demonstrates that fluids were being released from serpentinite at the time of diatreme emplacement (Smith, 2010). These observations are consistent with general P-T conditions of serpentinite dehydration, which match those of the diatreme source region (e.g., Usui et al., 2003; Ulmer & Trommsdorff, 2009; Smith, 2013). Large volumes of fluid can be stored in serpentinite in the slab mantle formed during hydration along ocean floor faults (e.g., Ranero et al., 2003). As the Farallon slab foundered into the asthenosphere, as is thought to have occurred between 40 and 20Ma (Coney & Reynolds, 1977; Humphreys, 1995; Humphreys et al., 2003; Humphreys, 2009; Levander et al., 2011; Cather et al., 2008), dehydrating serpentinite would have produced exceptionally large volumes of fluid. Models of diatreme emplacement also invoke dehydration of serpentinized mantle in response to minette intrusion, offering another possible fluid production mechanism. Lastly, the volume of hydration of the Colorado Plateau mantle (i.e. SUM matrix, antigorite peridotite xenoliths, etc.) requires a large fluid volume that would be difficult to produce with a less voluminous fluid source (e.g., Hacker, 2008; Marshall et al., 2017). Based on these lines of evidence, we consider a serpentinite-derived fluid the most likely source of the low- δ^{18} O garnet rims (Fig. 9).

Sources of heterogeneity beneath the Colorado Plateau

As noted in the results, a low- δ^{18} O rim zone is only preserved in one of the analyzed garnets in sample 12-97-45 (Fig. 5). While an intermediate zone is preserved in both garnets, this zone shows no change in isotopic composition from the core, consistent with closed-system garnet growth (Fig. 5a and 5b). Based upon the universal distribution of anhedral zone boundaries and crystal shapes, including embayments, and evidence of REE mobilization in monazite from other eclogite xenoliths, garnet resorption is the preferred explanation for the heterogeneous spatial distribution of the low- δ^{18} O zone (e.g., Fig. 5b; Schulze *et al.*, 2015). Resorption of garnet could have been driven by the abrupt increase in temperature or decrease in pressure associated with diatreme emplacement and already invoked to explain the pseudomorphic (and in some cases incomplete; Usui *et al.*, 2003) replacement of lawsonite by acicular zoisite aggregates (Helmstaedt & Doig, 1975; Smith & Zientek, 1979; Usui *et al.*, 2003; Usui *et al.*, 2006). The textural complexities of this sample, particularly in the morphology of the low- δ^{18} O rim zones points to a complex interrelation between fluid infiltration, growth and dissolution.

In contrast to the other three samples in this study, isotopic zonation and low- δ^{18} O rims are absent from both garnets in sample 12-97-53 (Fig. 6 and 9). Yet, even in the absence of isotopic evidence for fluid interaction, healed fracturing throughout the garnet cores reflect some amount of fluid-rock interaction (Fig. 6, Table 2). The isotopic homogeneity of garnets in 12-97-53 in the presence of evident fluid interaction can be explained in several ways. The first is that fluids infiltrating this xenolith suite were sourced from multiple locations (e.g., slab serpentinite and altered oceanic crust) and those interacting with 12-97-53 were fortuitously similar in isotopic composition. This is consistent with the uniform ages but variable chemistry observed in monazite by Schulze *et al.* (2015) and attributed to heterogeneous "Great Hydration" fluids, but is inconsistent with the convergence in δ^{18} O values in other samples in this study (Fig. 9).

Another explanation is that healed fracturing is the result of locally-derived fluid infiltration during prograde subduction which would account for the diffuseness of the fractures relative to the other samples. Sample 12-97-53 could then have been protected from later "Great Hydration" metasomatism by low permeability or a position isolated from fluid conduits. Precedent for this type of metasomatic heterogeneity is established by previous oxygen isotope studies of mantle xenoliths. Huang *et al.* (2014) observed δ^{18} O variations of ~2.5% at the thin section-scale between different domains of an eclogite xenolith from the Roberts Victor kimberlite, South Africa. Lastly, as with 12-97-45-B, resorption of garnet during diatreme emplacement could have removed garnet rims grown during late fluid-rock interaction, leaving only the healed fracture as evidence of this fluid influx. Irregular and truncated grain and zone boundaries in these garnets are evidence that garnet resorption took place, but the lack of garnets preserving relict rims precludes a definitive statement on the origin of isotopic homogeneity in these garnets. However, sample 12-97-53 stands as a further example of the textural complexities resulting from fluid processes active beneath the Colorado Plateau.

Atoll garnet

While atoll garnets are present in many eclogite xenoliths in the Colorado Plateau, sample 12-83-24 stands out for the presence of atoll garnet textures that are overgrown by later garnet (Fig. 3; e.g., Helmstaedt et al., 1972; Smith & Zientek, 1979). Garnet 12-83-24-A is dominated by a patchwork of garnet compositions showing no typical concentric zoning patterns, however in the core (and in the core of other garnets in this sample; Fig. 3c), a single homogeneous zone preserves an atoll-like shape. This atoll zone (1 in Fig. 7b) has a distinctly higher δ^{18} O value than the patchwork of zones that make up the rest of the garnet (Fig. 7). In the 12-97 samples where zoning is concentric, the highest- δ^{18} O core represents adoption of the protolith signature and

lower values in the rims record later fluid interaction. If we apply this interpretive method here, it is the incomplete atoll zone, and only concentric remnant, that represents the earliest growth in 12-83-24, and the lower- δ^{18} O patchwork core and rim zones that are later growth. These textural and δ^{18} O patterns are best explained as an atoll garnet overgrown by later garnet growth. The presence of preserved core material and euhedral outer edges in some atoll garnets from 12-83-24 (e.g., Fig. 3c) and in other studies is consistent with formation by initial skeletal growth of garnet (Smith & Zientek, 1979; Robyr et al., 2014). The presence of healed fracturing in the preserved atoll suggests that fluid played a role in the later overgrowth of the patchwork rim and core garnet (Fig. 7c). The process by which the later patchwork zones grew is still unclear, however Smith & Zientek (1979) proposed that rapid growth with slow diffusion was responsible for other examples of complex zoning in NVF eclogite xenoliths, and has been invoked for patchy zoning in Cr from orogenic garnet (Fig. 7c; e.g., Yang & Rivers, 2001; Angiboust et al., 2014). What the growth of these patchwork zones and the initial formation of the atoll can tell us about the fluid history of this sample is unclear, but these textural features clearly set it apart from the others in this study.

Pre-emplacement residence time

One of the controversies around the extent of Farallon-age mobilization and recrystallization of these eclogite xenoliths stems from their Proterozoic zircon ages (Smith *et al.*, 2004; Usui *et al.*, 2006; Malik *et al.*, 2017). Sharp prograde major element zone boundaries in garnet have been interpreted as evidence of Farallon-age subduction zone transport, as diffusive resetting would have erased any zoning formed during Proterozoic accretion (e.g., Smith & Zientek, 1979; Helmstaedt & Schulze, 1988; Smith, 2020). We used modeling of <20µm diffusion profiles at zone boundaries and healed fractures in garnets from the 12-97 samples to place quantitative

constraints on the timing of garnet fracture healing and rim growth relative to diatreme emplacement.

For garnet rims that record evidence of fluid infiltration, best fit models for the peak temperature and pressure (620°C at 3.7GPa; Hernández-Uribe & Palin, 2019) of the eclogite xenoliths produce durations of 32 to 190 thousand years between fluid infiltration and diatreme emplacement (Fig. 8 and 10, Table 3). If the minimum and maximum uncertainty bounds of the temperature estimate are considered (±50°C; Hernández-Uribe & Palin), durations for these low- δ^{18} O rims expand to 5000 years to 5Myr (Table 3). This strongly suggests a temporal link between low- δ^{18} O garnet growth driven by serpentinite-derived fluid infiltration, and diatreme emplacement. These short timescales are also comparable to the ~3Ma spread in monazite ages found by Schulze et al. (2015) and proposed as the duration of the "Great Hydration" fluid influx (Fig. 10). Results from healed fractures in sample 12-97-45 are similar in duration to low- δ^{18} O garnet rims (48 to 130 thousand years; Table 3), however the healed fracture from 12-97-11 preserves a longer duration (480 thousand years; Table 3). This suggests that healed fractures in some garnets are temporally associated with formation of low- δ^{18} O garnet and the "Great Hydration", while others may have formed during subduction (e.g., Broadwell et al., 2019). The garnet 12-97-53-A rim zone also preserves a longer duration of 320 thousand years (and up to 13 Myr) between rim growth and diatreme emplacement. This longer duration is consistent with the absence of low- δ^{18} O garnet rims and supports the idea that any "Great Hydration"-related garnet was resorbed (Table 3; Fig. 6 and 10). Diffusion modeling results from low- δ^{18} O garnet rims establish a temporal link between fluid influx and diatreme emplacement and support models of a "Great Hydration". These temporal relationships suggest that fluid infiltration was not related to steady-state subduction, but instead the result of processes occurring immediately prior to

diatreme emplacement such as slab removal, massive dehydration of the foundering serpentinized slab mantle, and asthenospheric return flow (Fig. 10).

The presence of inherited garnet from Proterozoic accretion can be assessed from the maximum residence times produced by our models. Maximum residence times of 290,000 years to 13 million years were generated by our model using the lower bound of the uncertainty in peak temperature (570°C; Hernández-Uribe & Palin, 2019), with all but sample 12-97-53, which records no isotopic evidence of fluid infiltration, yielding residence times <7.6Myr (Fig. 10, Table 3). Our longest residence time is two orders of magnitude shorter, and the longest associated with low- δ^{18} O values is three orders of magnitude shorter, than the U-Pb zircon ages of the Proterozoic protolith (Smith et al., 2004; Malik et al., 2017). Because of the exponential dependence of diffusivity on temperature, our models robustly constrain the pre-emplacement residence times of the eclogites within the subduction zone. Cold storage at the base of the crust prior to Farallon subduction cannot realistically extend these durations as storage conditions would have been significantly hotter prior to subduction. Thus, the modeled residence times, particularly those associated with low- δ^{18} O garnet, rule out the possibility that any of the zoning preserved in our garnets was inherited from the Proterozoic and requires Farallon-age mobilization and fluid-infiltration as has been previously concluded (Smith, 2020).

Bias due to assumed initial profiles, off-center garnet sections and artificial profile smoothing due to analytical conditions (convolution effects) is in the direction of longer residence times making our estimates robust maximums. If the initial concentration profiles in our models were gradual instead of step functions less diffusion would be necessary to reach the measured profiles and our model would yield shorter residence time. Similarly, off-center garnet sections would produce artificially gradual profiles and our model would overestimate residence times. Convolution effects describe the overlapping activation volumes of closely-space electron

microprobe analyses and will act to artificially smooth measured profiles lengthening modeled residence times (e.g., Ganguly *et al.*, 1988). With the given inputs, the upper bound of our ranges can be considered to be a definitive maximum (Table 3).

Implications for a "Great Hydration" and Colorado Plateau uplift

The eclogite xenoliths analyzed in this study point towards a complex fluid history beneath the Colorado Plateau recorded in intra-crystalline $\delta^{18}O$ and cation zoning in garnet. Here we will synthesize these findings with almost five decades of research on NVF xenoliths to present a model of the lithospheric evolution over the final 10Myr before diatreme emplacement.

Garnet rims with low- δ^{18} O values in this study record infiltration of a serpentinite-derived fluid sourced from the lithospheric mantle of the Farallon slab. Shifts in δ^{18} O away from pristine mantle values in peridotite xenoliths also resulted from interaction with a low- δ^{18} O slab serpentinite-derived fluid (Marshall *et al.*, 2017). All isotopically zoned garnets in this study converge to the same lower- δ^{18} O value, a value comparable to peridotite xenoliths, suggesting that a single fluid source, possibly a single period of fluid influx, is recorded in all these xenoliths (Fig. 9). In addition to the locally pervasive distribution of this fluid influx preserved in Moses Rock xenoliths, this low- δ^{18} O signature is present in xenoliths from Green Knobs diatreme over 100km away (Marshall *et al.*, 2017). Together with the dominance of SUM in all NVF diatremes, this common low- δ^{18} O isotopic signature suggests the spatial distribution of this fluid influx was of a comparable scale to the NVF, and potentially the Colorado Plateau or greater (e.g., Facer *et al.*, 2009). The stable isotope constraints from eclogite in this study and peridotite xenoliths from previous investigations suggest a large-scale serpentinite-derived fluid influx hydrated significant portions of the mantle beneath the Colorado Plateau.

Diffusion modeling of low-δ¹⁸O garnet zones suggests the timing of fluid influx was likely within 200 thousand years (and firmly within 5 Myr) of diatreme emplacement across all eclogite xenoliths. This limited range in residence time for low- δ^{18} O garnet zones suggests this fluid infiltration can be considered as a single, roughly contemporaneous "Great Hydration" event (Fig. 10, Table 3). Schulze et al. (2015) first proposed this single "Great Hydration" based on metasomatic monazite ages in Moses Rock eclogite xenoliths with a spread of 3Myr. They also observed that the ages of ~28Ma overlapped with estimates of diatreme emplacement and minette eruption that ranged from 21 to 30Ma (e.g., Naeser, 1971; Helmstaedt & Doig, 1975; Roden et al., 1979; Laughlin et al., 1986; Nowell, 1993; Smith et al., 2004). A similar age population between ~20 and 35Ma is also found in U-Pb zircon and Sm-Nd garnet geochronology across NVF eclogite xenoliths and require fluid to catalyze recrystallization (Wendlandt et al., 1996; Usui et al., 2003; Smith et al., 2004). The overlap between ages of diatreme emplacement and fluid-presence in eclogites supports our diffusion modeling results that fluid influx occurred as a single "Great Hydration" and was temporally related to diatreme emplacement.

Diffusion chronometry of subduction-derived peridotite xenoliths constrains the processes occurring in the diatreme source region between the influx of serpentinite-derived fluid and diatreme emplacement (Smith, 2010). Forsterite-rich olivine grown during chlorite breakdown in response to a thermal pulse (>800°C) yields residence times of <1700 years prior to emplacement (Smith, 2010). This thermal pulse is interpreted to be the result of minette magma intrusion into the diatreme source region and could have produced the volatiles thought to drive diatreme emplacement as gas-solid mixtures (e.g., McGetchin & Silver, 1970; Smith, 2010).

The direct connection between fluid influx and diatreme emplacement based on data from eclogite xenolith garnets presented here, and supporting evidence from similar eclogite and

peridotite xenoliths across the NVF, allow us to formulate a chronology of events immediately prior, and up to, diatreme emplacement. At approximately 28±1.5Ma and within <200 thousand years of diatreme emplacement, massive quantities of serpentinite-derived fluids from the mantle lithosphere of the Farallon plate infiltrated the NVF diatreme source region. This fluid influx grew garnet rims and monazite in underplated eclogites, and antigorite and chlorite in mantle peridotites, and recrystallized mantle olivine. Within 200 thousand years (and <1700 years prior to diatreme emplacement), minette magma intruded the source region destabilizing lawsonite and garnet in the eclogites, and dehydrating chlorite and antigorite to form forsterite-rich olivine rims in mantle peridotites. The volatiles given off by chlorite and antigorite dehydration created an unstable volatile and serpentinite mixture that then erupted as SUM within 1700 years.

The best mechanism to produce the temporal, spatial and geochemical characteristics of the "Great Hydration" fluid influx and subsequent thermal pulse and diatreme emplacement is through foundering of the Farallon slab. Inferred timing of slab foundering from 40 to 20Ma overlaps with monazite, garnet and zircon ages from eclogite xenoliths, emplacement ages of the diatremes, and with the timing of fluid influx and a late thermal pulse from diffusion modeling, favoring a role for foundering in these processes (e.g., Naeser, 1971; Coney & Reynolds, 1977; Roden *et al.*, 1979; Humphreys, 1995; Wendlandt *et al.*, 1996; Usui *et al.*, 2003; Cather *et al.*, 2008; Smith, 2010; Schulze *et al.*, 2015). Sub-vertical sinking of the Farallon slab into the asthenosphere would have led to widespread slab heating, dehydrating the remaining serpentinite nearly simultaneously over a large area. Slab foundering would have also been followed by asthenospheric return flow that could have driven minette intrusion and dehydration within the recently hydrated mantle necessary for diatreme emplacement.

The evidence across four eclogite xenoliths for a single common fluid influx strongly supports the role of a "Great Hydration" in Colorado Plateau uplift. A single fluid release of this

scale could add significantly to the estimated 13% serpentinization necessary to uplift the plateau to its current position (Schulze *et al.*, 2015). Further study of the NVF eclogite xenoliths as well as other lithologies could shed more light on the spatial and temporal distribution of the "Great Hydration" as well as its relationship with slab detachment and minette intrusion. The discovery of oxygen isotope zoning in these xenoliths opens the possibility for a more detailed record of fluid interaction and mantle metasomatism beneath the Colorado Plateau, and, while the NVF xenoliths are unusual, the reevaluation of assumed isotopic homogeneity in some mantle xenoliths may be warranted.

FUNDING

This work was supported by the National Science Foundation (NSF) [EAR 1249778 to F.Z.P]. The electron microprobe and electron microscopes used in this work were funded by the NSF [EAR 96-28196, EAR 99-11352, CCLI 00-87895]. WiscSIMS is supported by the NSF [EAR-1355590, EAR-1658823] and the University of Wisconsin, Madison.

ACKNOWLEDGEMENTS

The authors are grateful to Gordon Moore for assistance with electron microprobe analyses.

Constructive reviews by E. Marshall, I.-B. Radu, E. Humphreys, an anonymous reviewer and editorial handling by G. Wörner are gratefully acknowledged. The Navajo Nation and the Dennehotso Chapter are thanked for permission to collect these samples and publish the results. Field work on the Navajo Nation was conducted under a permit from the Navajo Nation Minerals Department. Any persons wishing to conduct geologic investigations on the Navajo Nation must first apply for, and receive, a permit from the Navajo Nation Minerals Department, P.O. Box 1910, Window Rock, Arizona 86515, telephone # (928) 871-6587.

REFERENCES

- Alt, J. C., Muehlenbachs, K. & Honnorez, J. (1986). An oxygen isotopic profile through the upper kilometer of the oceanic crust, DSDP Hole 504B. *Earth and Planetary Science Letters* **80**, 217-229.
- Angiboust, S., Pettke, T., De Hoog, J. C. M., Caron, B. & Oncken, O. (2014). Channelized fluid flow and eclogite-facies metasomatism along the subduction shear zone. *Journal of Petrology* **55**, 883-916.
- Broadwell, K. S., Locatelli, M., Verlaguet, A., Agard, P. & Caddick, M. J. (2019). Transient and periodic brittle deformation of eclogites during intermediate-depth subduction. *Earth and Planetary Science Letters* **521**, 91-102.
- Carlson, W. D. (2006). Rates of Fe, Mg, Mn, and Ca diffusion in garnet. *American Mineralogist* **91**, 1-11.
- Cartwright, I. & Barnicoat, A. C. (1999). Stable isotope geochemistry of Alpine ophiolites: A window to ocean-floor hydrothermal alteration and constraints on fluid-rock interaction during high-pressure metamorphism. *International Journal of Earth Sciences* **88**, 219-235.
- Cather, S. M., Connell, S. D., Chamberlin, R. M., McIntosh, W. C., Jones, G. E., Potochnik, A. R., Lucas, S. G. & Johnson, P. S. (2008). The Chuska erg: Paleogeomorphic and paleoclimatic implications of an Oligocene sand sea on the Colorado Plateau. *GSA Bulletin* **120**, 13-33.
- Chakraborty, S. & Ganguly, J. (1992). Cation diffusion in aluminosilicate garnets: experimental determination in spessartine-almandine diffusion couples, evaluation of effective binary diffusion coefficients, and applications. *Contributions to Mineralogy and Petrology* 111, 74-86.
- Clayton, R. N., Goldsmith, J. R., Karel, K. J., Mayeda, T. K. & Newton, R. C. (1975). Limits on the effect of pressure on isotopic fractionation. *Geochimica et Cosmochimica Acta* **39**, 1197-1201.
- Coney, P. J. & Reynolds, S. J. (1977). Cordilleran Benioff zones. *Nature* 270, 403-406.
- Crank, J. (1975). *The mathematics of diffusion*. Oxford University Press.
- Davis, G. H. & Bump, A. P. (2009). *Structural geologic evolution of the Colorado Plateau*. In: Mahlburg Kay, S., Ramos, V. A. & Dickinson, W. R. (eds) *Backbone of the Americas:*

- Shallow subduction, plateau uplift, and ridge and terrane collision. Geological Society of America, Geological Society of America Memoir **204**, 99-124.
- Dickinson, W. R. & Snyder, W. S. (1978). Plate tectonics of the Laramide orogeny. In: Matthews, V. (ed) Laramide folding associated with basement block faulting in the western United States. Geological Society of America, Geological Society of America Memoir 151, 355-366.
- Dickinson, W. R. (2004). Evolution of the North American Cordillera. *Annual Reviews in Earth and Planetary Science* **32**, 13-45.
- Eiler, J. (2001). Oxygen isotope variations of basaltic lavas and upper mantle rocks. In: Valley, J. W. & Cole, D. R. (eds) Stable isotope geochemistry. Mineralogical Society of America, Reviews in Mineralogy and Geochemistry 43, 319-364.
- Engebretson, D. C., Cox, A. & Gordon, R. G. (1985). Relative motions between oceanic and continental plates in the Pacific Basin. *Geological Society of American Special Paper* **206**, 1-59.
- Errico, J. C., Barnes, J. D., Strickland, A. & Valley, J. W. (2013) Oxygen isotope zoning in garnets from Franciscan eclogite blocks: Evidence for rock-buffered fluid interaction in the mantle wedge. *Contributions to Mineralogy and Petrology* **166**, 1161-1176.
- Facer, J., Downes, H. & Beard, A. (2009). In situ Serpentinization and Hydrous Fluid Metasomatism in Spinel Dunite Xenoliths from the Bearpaw Mountains, Montana, USA. *Journal of Petrology* **50**, 1443-1475.
- Flowers, R. M., Wernicke, B. P. & Farley, K. A. (2008). Unroofing, incision, and uplift history of the southwestern Colorado Plateau from apatite (U-Th)/He thermochronometry. *GSA Bulletin* **120**, 571-587.
- Früh-Green, G. L., Scambelluri, M. & Vallis, F. (2001). O-H isotope ratios of high pressure ultramafic rocks: Implications for fluid sources and mobility in the subducted hydrous mantle. *Contributions to Mineralogy and Petrology* **141**, 145-159.
- Ganguly, J., Bhattacharya, R. N., Chakraborty, S. (1988). Convolution effect in the determination of compositional profiles and diffusion coefficients by microprobe step scans. *American Mineralogist* **73**, 901-909.
- Ganguly, J., Cheng, W. & Chakraborty, S. (1998). Cation diffusion in aluminosilicate garnets: experimental determination in pyrope-almandine diffusion couples. *Contributions to Mineralogy and Petrology* **131**, 171-180.
- Ganguly, J. (2010). Cation diffusion kinetics in aluminosilicate garnets and geological applications. In: Zhang, Y. & Cherniak, D. J. (eds) Diffusion in minerals and melts. Mineralogical Society of America, Reviews in Mineralogy & Geochemistry 72, 559-601.

- Gregory, R. T. & Taylor, H. P. Jr. (1981). An oxygen isotope profile in a section of Cretaceous oceanic crust, Samail Ophiolite, Oman: Evidence for δ¹⁸O buffering of the oceans by deep (>5km) seawater-hydrothermal circulation at mid-ocean ridges. *Journal of Geophysical Research* **86**, 2737-2755.
- Hacker, B. R. (2008). H₂O subduction beyond arcs. Geochemistry, Geophysics, Geosystems 9.
- Helmstaedt, H., Anderson, O. L. & Gavasci, A. T. (1972). Petrofabric studies of eclogite, spinel-websterite, and spinel-lherzolite xenoliths from kimberlite-bearing breccia pipes in southeastern Utah and northeastern Arizona. *Journal of Geophysical Research* 77, 4350-4365.
- Helmstaedt, H. & Doig, R. (1975). Eclogite nodules from kimberlite pipes of the Colorado Plateau Samples of subducted Franciscan-type oceanic lithosphere. *Physics and Chemistry of the Earth* **9**, 95-112.
- Helmstaedt, H. & Schulze, D. J. (1988). *Eclogite-facies ultramafic xenoliths from Colorado Plateau diatreme breccias: Comparison with eclogites in crystal environments, evaluation of the subduction hypothesis, and implications for eclogite xenoliths from diamondiferous kimberlites*. In: Smith, D. (ed.) *Eclogites and Eclogite-facies Rocks*. Elsevier, 387-450.
- Helmstaedt, H. H. & Schulze, D. J. (1991). Early to mid-Tertiary inverted metamorphic gradient under the Colorado Plateau: Evidence from eclogite xenoliths in ultramafic microbreccias, Navajo Volcanic Field. *Journal of Geophysical Research* **96**, 13225-13235.
- Hernández-Uribe, D. & Palin, R. (2019). Catastrophic shear-removal of subcontinental lithospheric mantle beneath the Colorado Plateau by the subducted Farallon slab. *Scientific Reports* **9**.
- Huang, J.-X., Griffin, W. L., Gréau, Y., Pearson, N. J., O'Reilly, S. Y., Cliff, J. & Martin, L. (2014). Unmasking xenolithic eclogites: Progressive metasomatism of a key Roberts Victor sample. *Chemical Geology* **364**, 56-65.
- Huangfu, P., Wang, Y., Cawood, P. A., Li, Z.-H., Fan, W. & Gerya, T. V. (2016). Thermomechanical controls of flat subduction: Insights from numerical modeling. *Gondwana Research* **40**, 170-183.
- Humphreys, E. (1995). Post-Laramide removal of the Farallon slab, western United States. *Geology* **23**, 987-990.
- Humphreys, E., Hessler, E., Dueker, K., Farmer, G. L., Ersley, E. & Atwater, T. (2003). How Laramide-age hydration of North American lithosphere by the Farallon slab controlled subsequent activity in the western United States. *International Geology Review* **45**, 575-595.

- Humphreys, E. (2009). Relation of flat subduction to magmatism and deformation in the western United States. In: Mahlburg Kay, S., Ramos, V. A. & Dickinson, W. R. (ed) Backbone of the Americas: Shallow subduction, plateau uplift, and ridge and terrane collision. Geological Society of America, Geological Society of America Memoir 204, 85-98.
- Ickert, R. B. & Stern, R. A. (2013). Matrix corrections and error analysis in high-precision SIMS ¹⁸O/¹⁶O measurements of Ca-Mg-Fe garnet. *Geostandards and Geoanalytical Research* **37**, 429-448.
- Jollands, M. C., Hanger, B. J., Yaxley, G. M., Hermann, J. & Kilburn, M. R. (2018). Timescales between mantle metasomatism and kimberlite ascent indicated by diffusion profiles in garnet crystals from peridotite xenoliths. *Earth and Planetary Science Letters* **481**, 143-153.
- Jones, C. H., Mahan, K. H., Butcher, L. A., Levandowski, W. B. & Farmer, G. L. (2015). Continental uplift through crustal hydration. *Geology* **43**, 55-358.
- Kita, N. T., Ushikubo, T., Fu, B. & Valley, J. W. (2009). High precision SIMS oxygen isotope analysis and the effect of sample topography. *Chemical Geology* **264**, 43-57.
- Laughlin, A. W., Aldrich, M. J. Jr., Shafiqullah, M. & Husler, J. (1986). Tectonic implications of the age, composition, and orientation of lamprophyre dikes, Navajo Volcanic Field, Arizona. *Earth and Planetary Science Letters* **76**, 361-374.
- Levander, A., Schmandt, B., Miller, M. S., Liu, K., Karlstrom, K. E., Crow, R. S., Lee, C.-T., A. & Humphreys, E. D. (2011). Continuing Colorado Plateau uplift by delamination-style convective lithospheric downwelling. *Nature* **472**, 461-466.
- Li, J.-L., Gao, J., Klemd, R., John, T. & Wang, X.-S. (2016). Redox processes in subducting oceanic crust recorded by sulfide-bearing high-pressure rocks and veins (SW Tianshan, China). *Contributions to Mineralogy and Petrology* **171**.
- Lipman P. W. (1992). *Magmatism in the Cordilleran United States; Progress and problems*. In: Burchfiel, B.C., Lipman, P. W. & Zoback M. L. (ed) *The Geology of North America: Vol. G-3, The Cordilleran Orogen: Conterminous U.S.* Geological Society of America, 481-514.
- Liu, L. & Gurnis, M. (2010). Dynamic subsidence and uplift of the Colorado Plateau. *Geology* **38**, 663-666.
- Malik, L., Schulze, D. J., Davis, D. W. & Helmstaedt, H. (2017). Age and origin of eclogite xenoliths from Navajo diatremes on the Colorado Plateau. AGU Fall Meeting, V13D 0409S, San Francisco, USA.
- Marshall, E. W., Barnes, J. D. & Lassiter, J. C. (2017). The role of serpentinite-derived fluids in metasomatism of the Colorado Plateau (USA) lithospheric mantle. *Geology* **45**, 1103-1106.

- Mattinson, C. G., Zhang, R. Y., Tsujimori, T. & Liou, J. G. (2004). Epidote-rich talc-kyanite-phengite eclogites, Sulu terrane, eastern China: P-T-fo2 estimates and the significance of the epidote-talc assemblage in eclogite. *American Mineralogist* **89**, 1772-1783.
- McGetchin, T. R. & Silver, L. T. (1970). Composition relations in minerals from kimberlite and related rocks in the Moses Rock Dike, San Juan County, Utah. *American Mineralogist* **55**, 1738-1771.
- McGetchin, T. R. & Silver, L. T. (1972). A crustal-upper mantle model for the Colorado Plateau based on observations of crystalline rock fragments in the Moses Rock Dike. *Journal of Geophysical Research* 77, 7022-7037.
- McGetchin, T. R., Smith, D., Ehrenberg, S. N., Roden, M. & Wilshire, H. G. (1977). Navajo kimberlites and minettes. *Second International Kimberlite Conference Field Excursion Guide, Santa Fe, NM*.
- Miller, J. A., Cartwright, I., Buick, I. S. & Barnicoat, A. C. (2001). An O-isotope profile through the HP-LT Corsican ophiolite, France and its implications for fluid flow during subduction. *Chemical Geology* **178**, 43-69.
- Naeser, C. W. (1971). Geochronology of the Navajo-Hopi diatremes, Four Corners Area. *Journal of Geophysical Research* **76**, 4978-4985.
- Nowell, G. M. (1993). Cenozoic potassic magmatism and uplift of the western United States. Ph.D. thesis, Open University, Milton Keynes, England.
- Page, F. Z., Fu, B., Kita, N. T., Fournelle, J., Spicuzza, M. J., Schulze, D. J., Viljoen, F., Basei, M. & Valley, J. W. (2007). Zircons from kimberlite: New insights from oxygen isotopes, trace elements, and Ti in zircon thermometry. *Geochimica et Cosmochimica Acta*, 71, 3887-3903.
- Page, F. Z., Kita, N. T. & Valley, J. W. (2010). Ion microprobe analysis of oxygen isotopes in garnets of complex chemistry. *Chemical Geology* **270**, 9-19.
- Page, F. Z., Essene, E. J., Mukasa, S. B. & Valley, J. W. (2014). A garnet-zircon oxygen isotope record of subduction and exhumation fluids from the Franciscan Complex, California. *Journal of Petrology* **55**, 103-131.
- Perkins, G. B., Sharp, Z. D. & Selverstone, J. (2006). Oxygen isotope evidence for subduction and rift-related mantle metasomatism beneath the Colorado Plateau-Rio Grande rift transition. *Contributions to Mineralogy and Petrology* **151**, 633-650.
- Putlitz, B., Matthews, A. & Valley, J. W. (2000). Oxygen and hydrogen isotope study of high-pressure metagabbros and metabasalts (Cyclades, Greece): Implications for the subduction of oceanic crust. *Contributions to Mineralogy and Petrology* **138**, 114-126.

- Quinn, R.J., Valley, J.W., Page, F.Z., & Fournelle, J.H. (2016) Accurate determination of ferric iron in garnets: *American Mineralogist* **101**, 1704–1707.
- Radu, I.-B., Harris, C., Moine, B. N., Costin, G. & Cotton, J.-Y. (2019). Subduction relics in the subcontinental lithospheric mantle evidence from variation in the δ¹⁸O value of eclogite xenoliths from the Kaapvaal craton. *Contributions to Mineralogy and Petrology*, **174**.
- Ranero, C. R., Morgan, J. P., McIntosh, K. & Reichert, C. (2003). Bending-related faulting and mantle serpentinization at the Middle America Trench. *Nature* **425**, 367-373.
- Riches, A. J. V., Ickert, R. B., Pearson, D. G., Stern, R. A., Jackson, S. E., Iskikawa, A., Kjarsgaard, B. A. & Gurney, J. J. (2016). *In situ* oxygen-isotope, major-, and trace-element constraints on the metasomatic modification and crustal origin of a diamondiferous eclogite from Roberts Victor, Kaapvaal Craton. *Geochimica et Cosmochimica Acta* 174, 345-359.
- Robyr, M., Darbellay, B. & Baumgartner, L. P. (2014). Matrix-dependent garnet growth in polymetamorphic rocks of the Sesia zone, Italian Alps. *Journal of Metamorphic Geology* **32**, 3-24.
- Roden, M. F., Smith, D. & McDowell, F. W. (1979). Age and extent of potassic volcanism on the Colorado Plateau. *Earth and Planetary Science Letters* **43**, 279-284.
- Roden, M. F. (1981). Origin of coexisting minette and ultramafic breccia, Navajo Volcanic Field. *Contributions to Mineralogy and Petrology* 77, 195-206.
- Roden, M. F. & Smith, D. (1971). Field geology, chemistry, and petrology of Buell Park minette diatreme, Apache County, Arizona. In: Meyer, H. O. A. & Boyd, F. R. (ed) Kimberlites, diatremes, and diamonds: Their geology, petrology, and geochemistry, Volume 15, American Geophysical Union, 364-381.
- Rubatto, D. & Angiboust, S. (2015). Oxygen isotope record of oceanic and high-pressure metasomatism: A P-T-time-deformation path of the Monviso eclogites (Italy). *Contributions to Mineralogy and Petrology* **170**, 1-16.
- Russell, A. K., Kitajima, K., Strickland, A., Medaris, L. G. Jr., Schulze, D. J. & Valley, J. W. (2013) Eclogite-facies fluid infiltration: Constraints from δ¹⁸O zoning in garnet. *Contributions to Mineralogy and Petrology* **165**, 103-116.
- Sahagian, D., Proussevitch, A. & Carlson, W. (2002). Timing of Colorado Plateau uplift: Initial constraints from vesicular basalt-derived paleoelevations. *Geology* **30**, 807-810.
- Saleeby, J. (2003). Segmentation of the Laramide Slab evidence from the southern Sierra Nevada region. *GSA Bulletin* **115**, 655-668.

- Scambelluri, M., Fiebig, J., Malaspina, N., Müntener, O. & Pettke, T. (2004). Serpentinite subduction: Implications for fluid processes and trace-element recycling. *International Geology Review* **46**, 595-613.
- Schulze D. J., Flemming, R. L., Shepard, P. H. M. & Helmstaedt, H. (2014). Mantle-derived guyanaite in a Cr-omphacitite xenolith from Moses Rock diatreme, Utah. *American Mineralogist* **99**, 1277-1283.
- Schulze, D. J., Davis, D. W., Helmstaedt, H. & Joy, B. (2015). Timing of the Cenozoic "Great Hydration" event beneath the Colorado Plateau: Th-Pb dating of monazite in Navajo volcanic field metamorphic eclogite xenoliths. *Geology* **43**, 727-730.
- Smart, K. A., Tappe, S., Simonetti, A., Simonetti, S. S., Woodland, A. B. & Harris, C. (2017). Tectonic significance and redox state of Paleoproterozoic eclogite and pyroxenite components in the Slave cratonic mantle lithosphere, Voyageur kimberlite, Arctic Canada. *Chemical Geology* **455**, 98-119.
- Smit, K. V., Stachel, T., Creaser, R. A., Ickert, R. B., DuFrane, S. A., Stern, R. A. & Seller, M. (2014). Origin of eclogite and pyroxenite xenoliths from the Victor kimberlite, Canada, and implications for Superior craton formation. *Geochimica et Cosmochimica Acta* 125, 308-337.
- Smith, D. & Levy, S. (1976). Petrology of the Green Knobs diatreme ad implications for the upper mantle below the Colorado Plateau. *Earth and Planetary Science Letters* **29**, 107-125.
- Smith, D. & Zientek, M. (1979). Mineral chemistry and zoning in eclogite inclusions from Colorado Plateau diatremes. *Contributions to Mineralogy and Petrology* **69**, 119-131.
- Smith, D. & Roden, M. F. (1981). Geothermometry and kinetics in a two-spinel peridotite nodule, Colorado Plateau. *American Mineralogist* **66**, 334-345.
- Smith, D. (1995). Chlorite-rich ultramafic reaction zones in Colorado Plateau xenoliths: Recorders of sub-Moho hydration. *Contributions to Mineralogy and Petrology* **121**, 185-200.
- Smith, D., Riter, J. C. A. & Mertzman, S. A. (1999). Water-rock interactions, orthopyroxene growth, and Si-enrichment in the mantle: Evidence in xenoliths from the Colorado Plateau, southwestern United States. *Earth and Planetary Science Letters* **165**, 45-54.
- Smith, D., Connelly, J. N., Manser, K., Moser, D. E., Housh, T. B., McDowell, F. W. & Mack, L. E. (2004). Evolution of the Navajo eclogites and hydration of the mantle wedge below the Colorado Plateau, southwestern United States. *Geochemistry Geophysics Geosystems* 5.
- Smith, D. & Griffin, W. L. (2005). Garnetite xenoliths and mantle-water interactions below the Colorado Plateau, southwestern United States. *Journal of Petrology* **46**, 1901-1924.

- Smith, D. (2010). Antigorite peridotite, metaserpentinite, and other inclusions within diatremes on the Colorado Plateau, SW USA: Implications for the mantle wedge during low-angle subduction. *Journal of Petrology* **51**, 1355-1379.
- Smith, D. (2013). Olivine thermometry and source constraints for mantle fragments in the Navajo Volcanic Field, Colorado Plateau, southwest United States: Implications for the mantle wedge. *Geochemistry Geophysics Geosystems* **14**.
- Smith, D. (2020). Trace elements in Cr-pyrope from the Navajo volcanic field of the Colorado Plateau, SW USA, and implications for the mantle wedge during low-angle subduction. *Lithos* **362-363**.
- Syracuse, E. M., van Keken, P. E. & Abers, G. A. (2010). The global range of subduction zone thermal models. *Physics of the Earth and Planetary Interiors* **183**, 73-90.
- Tao, R. B., Zhang, L. F., Stagno, V., Chu, X. & Liu, X. (2017). High-pressure experimental verification of rutile-ilmenite oxybarometer: Implications for the redox state of the subduction zone. *Science China Earth Sciences* 60, 1817-1825.
- Ulmer, P. & Trommsdorff, V. (1995). Serpentine stability to mantle depths and subduction-related magmatism. *Science* **268**, 858-861.
- Usui, T., Nakamura, E., Kobayashi, K., Maruyama, S. & Helmstaedt, H. (2003). Fate of the subducted Farallon plate inferred from eclogite xenoliths in the Colorado Plateau. *Geology* **31**, 589-592.
- Usui, T., Nakamura, E. & Helmstaedt, H. (2006). Petrology and geochemistry of eclogite xenoliths from the Colorado Plateau: Implications for the evolution of subducted oceanic crust. *Journal of Petrology* **47**, 929-964.
- Valley, J. W. (2003) *Oxygen isotopes in zircon*. In: Hanchar, J. M. and Hoskin, P. W. O. (eds) *Zircon*. Mineralogical Society of America, Reviews in Mineralogy and Geochemistry **53**, 343-385.
- Valley, J. W., Kitchen, N., Kohn, M. J., Niendorf, C. R. & Spicuzza, M. J. (1995). UWG-2, a garnet standard for oxygen isotope ratios: Strategies for high precision and accuracy with laser heating. *Geochimica et Cosmochimica Acta* **59**, 5223-5231.
- Valley, J. W., Kinny, P., Schulze, D. J. & Spicuzza, M.J. (1998). Zircon megacrysts from kimberlite: Oxygen isotope variability among mantle melts. *Contributions to Mineralogy and Petrology*, **133**, 1-11.
- Valley, J. W. & Kita, N. T. (2009). In situ oxygen isotope geochemistry by ion microprobe. Secondary Ion Mass Spectrometry in the Earth Sciences, Mineralogical Association of Canada, Short Course 41, 19-63.

- Vielzeuf, D., Veschambre, M. & Brunet, F. (2005a). Oxygen isotope heterogeneities and diffusion profile in composite metamorphic-magmatic garnets from the Pyrenees. *American Mineralogist* **90**, 463-472.
- Vielzeuf, D., Champenois, M., Valley, J. W., Brunet, F. & Devidal, J. L. (2005b). SIMS analyses of oxygen isotopes: Matrix effects in Fe-Mg-Ca garnets. *Chemical Geology* **223**, 208-226.
- Wang, X.-L., Coble, M. A., Valley, J. W., Shu, X.-J., Kitajima, K., Spicuzza, M. J. & Sun, T. (2014). Influence of radiation damage on Late Jurassic zircon from southern China: Evidence from *in situ* measurements of oxygen isotopes, laser Raman, U-Pb ages, and trace elements. *Chemical Geology* **389**, 122-136.
- Wendlandt, E., DePaolo, D. J. & Baldridge, W. S. (1993). Nd and Sr isotope chronostratigraphy of Colorado Plateau lithosphere: Implications for magmatic and tectonic underplating of the continental crust. *Earth and Planetary Science Letters* **116**, 23-43.
- Wendlandt, E., DePaolo, D. J. & Baldridge, W. S. (1996). Thermal history of Colorado Plateau lithosphere from Sm-Nd mineral geochronology of xenoliths. *GSA Bulletin* **108**, 757-767.
- Yang, P. & Rivers, T. (2001). Chromium and manganese zoning in pelitic garnet and kyanite: Spiral, overprint, and oscillatory (?) zoning patterns and the role of growth rate. *Journal of Metamorphic Geology* **19**, 455-474.

- **Figure 1.** A map of the southwestern USA showing the location of Moses Rock in relation to the Colorado Plateau and Navajo Volcanic Field. Though uplifted ~1.8km, the Colorado Plateau remains largely undeformed relative to the neighboring tectonic provinces (Basin and Range, Rio Grande Rift and Rocky Mountains, modified from Schulze *et al.*, 2015).
- **Figure 2.** Photomicrographs in plane polarized light of (a) sample 12-97-53 and (b) sample 12-83-24 representative of the textural and mineralogical contrast between the 12-97 samples and sample 12-83-24. In 12-97-53 garnet is found as large and discrete crystals, while in 12-83-24 garnet forms elongate aggregates. Foliation is more pronounced in 12-97-53 and defined by zoisite which is absent from 12-83-24. (Grt = garnet; Omp = omphacite; Zo = zoisite; Rt = rutile; Ap = apatite)
- **Figure 3.** High-contrast back-scattered electron images from samples 12-97-11 (a) and (b) and 12-83-24 (c) illustrating a variety of atoll garnet textures from Moses Rock eclogite xenoliths. Garnet cores in (a and b) are largely filled with omphacite (appears black). In (c), the garnet has been recrystallized filling the euhedral atoll (bright zone) with new garnet (various grey zones).
- **Figure 4.** Major element and oxygen isotope compositions of garnets from sample 12-97-11. High-contrast back-scattered electron images of garnets: (a) 12-97-11-A and (b) 12-97-11-B, showing high- δ^{18} O cores and low- δ^{18} O rims. These core values preserve altered upper oceanic crust protolith signatures while deviations at the rim record infiltration of a serpentinite-derived fluid. Heterogeneity in cation composition can be seen in the bright annulus just inside of the low- δ^{18} O rim in (a) relative to the prograde zoning visible in (b). Ovals mark oxygen analysis pits and are color-coded for their associated δ^{18} O zone. Pits are labeled with their associated δ^{18} O value. White flecks are residual gold coating. A traverse for cation composition and δ^{18} O from garnet 12-97-11-B is marked by a blue bar A-A' in (b) and associated analyses are plotted (c). Shaded bands in (c) mark different grayscale zones visible in the associated BSE image (b).
- **Figure 5.** Major element and oxygen isotope compositions of garnets from sample 12-97-45. High-contrast back-scattered electron images of garnets: (a) 12-97-45-A and (b) 12-97-45-B, showing the heterogeneous preservation of the lowest- δ^{18} O zone. Embayed garnet rims suggest this feature is the result of garnet resorption rather than heterogeneous distribution of the serpentinite-derived fluid. Linear features cross-cutting the cores of both (a) and (b) are fractures healed with new garnet during fluid influx. Ovals mark oxygen isotope analysis pits labeled with their associated δ^{18} O value and color-coded for their zone. Cation traverse A-A' is marked with a blue bar in (a) and associated analyses are plotted in (c). Shaded bands in (c) refer to grayscale zones visible in the associated BSE image (a).
- **Figure 6.** Oxygen isotope compositions of garnets from sample 12-97-11. High-contrast back-scattered electron images of garnets: (a) 12-97-53-A and (b) 12-97-53-B, showing $\delta^{18}O$ homogeneity but cation zoning and healed fractures indicating changing metamorphic conditions and fluid interaction during growth. The abundance of embayments in the garnet rims suggest that lack of preservation may explain the absence of a low- $\delta^{18}O$ rim zone in this sample. Ovals mark oxygen isotope analysis pits labeled with their associated $\delta^{18}O$ values.
- **Figure 7.** Major element and oxygen isotope compositions of garnets from sample 12-83-24. (a) High-contrast back-scattered electron image of garnet 12-83-24-A showing the complex zoning

characteristic of this sample. The high- $\delta^{18}O$ values in the bright zone is interpreted to represent first garnet growth with later diffusion-limited recrystallization forming the complex intergrowths in the core and rim. Ovals mark $\delta^{18}O$ analysis pits labeled with their associated $\delta^{18}O$ value and color-coded for their $\delta^{18}O$ zone. The cation traverse plotted in (b) is marked by the blue bar from A to A'. (b) Cation and $\delta^{18}O$ analyses along traverse A-A' are plotted with other $\delta^{18}O$ values assigned a position along the traverse based upon cation chemistry and marked with an "x". Numbers and shaded bands identify zones differentiated by oxygen isotope and cation analyses. (c) Detail of the traverse portion of (A) with the relict atoll outlined. The fine-scale, complex zoning in the later low- $\delta^{18}O$ garnet is clearly visible as is the healed fracturing in the relict atoll.

Figure 8: Back-scattered electron images and representative multi-component diffusion model results for garnet rim (12-97-45-A outside rim) (a) and (b), and healed fracture (12-97-45-B fracture) (c) and (d) at 620°C. In (a) and (c), black bars mark the position of measured traverses plotted in (b) and (d), respectively. Plotted lines in (b) and (d) are a range of diffusion models at 620°C considered good fits to the measured profiles, based on visual assessment. Variability in the models in (b) close to the zone boundary are the result of a complex initial geometry. Multiple initial steps in concentration were necessary to maximize the fit of the model to the measured data. Abbreviations are: Alm = almandine, Grs = grossular, Pyp = pyrope, Sps = spessartine.

Figure 9: Compilation of oxygen isotope profiles across garnets in this study with core-to-rim distances normalized for comparison. Low- δ^{18} O zones in all samples that preserve zoning converge at values of ~6.5% suggesting a shared history of fluid infiltration. Based on tectonic, trace element and stable isotope arguments, this fluid is likely derived from serpentinite in the Farallon lithospheric mantle (Marshall *et al.*, 2017). Higher δ^{18} O values in all samples are consistent with an altered oceanic crust protolith suggesting closed system growth during prograde subduction. Mantle garnet (with 2SD uncertainty, fine dashed lines) and serpentinite (shaded region) are plotted for comparison. Analyses from sample 12-83-24 were assigned positions based on atoll and overgrowth textures.

Figure 10: Diffusion model results from all samples, including those recording the timing of low- δ^{18} O fluid infiltration. Best fit durations from rim zone boundaries are plotted as circles and healed fractures are plotted as diamonds. Error bars show model results incorporating uncertainty in the peak temperature estimate (±50°C; Hernández-Uribe & Palin, 2019). Short timescales between fluid infiltration and diatreme emplacement recorded by low-δ¹⁸O garnet rims are in agreement with geochronologic evidence of a "Great Hydration". The lack of isotopic evidence for fluid infiltration in the rim of garnet 12-97-53-A suggests it does not preserve evidence of the Great Hydration consistent with the longer durations from diffusion modeling. Maximum duration of a late thermal pulse calculated from Fe-Mg diffusion in olivine in a dunite xenolith is marked by the black bar (Smith, 2010). Two standard deviation range of monazite Th-Pb ages dating the "Great Hydration" are plotted in the blue bar (n=55, Schulze et al., 2015). Inferred timing for foundering of the Farallon slab beneath the Colorado Plateau is plotted as the red bar (Coney & Reynolds, 1977; Humphreys, 1995; Humphreys et al., 2003; Humphreys, 2009; Levander et al., 2011; Cather et al., 2008). Timescales derived from diffusion modeling are comparable to the duration of the Great Hydration and foundering of the Farallon plate suggesting a link between the fluid infiltration recorded in garnet rims and monazite growth, and foundering-induced serpentinite dehydration.